TIMING OBSERVATIONS FROM ROSSI X-RAY TIMING EXPLORER (RXTE)

A THESIS SUBMITTED TO
THE GRADUATE SCHOOL OF NATURAL AND APPLIED SCIENCES
OF
THE MIDDLE EAST TECHNICAL UNIVERSITY

BY

ELİF BEKLEN

IN PARTIAL FULFILLMENT OF THE REQUIREMENTS FOR THE DEGREE OF

MASTER OF SCIENCE

IN

THE DEPARTMENT OF PHYSICS

JANUARY 2004

Approval of the Graduate School of Natural and Applied Sciences.

Prof. Dr. Canan Özgen
Director

I certify that this thesis satisfies all the requirements as a thesis for the degree of Master of Science.

Prof. Dr. Sinan Bilikmen
Head of Department

This is to certify that we have read this thesis and that in our opinion it is fully adequate, in scope and quality, as a thesis for the degree of Master of Science.

Prof. Dr. Altan Baykal
Supervisor

Examining Committee Members

Prof. Dr. Altan Baykal

Prof. Dr. Ali Alpar

Prof. Dr. Halil Kırbıyık

Prof. Dr. Nilgün Kızıloğlu

Assist. Prof. Dr. Sinan Kaan Yerli

ABSTRACT

TIMING OBSERVATIONS FROM ROSSI X-RAY TIMING EXPLORER (RXTE)

BEKLEN, ELİF
M.S., Department of Physics
Supervisor: Prof. Dr. Altan Baykal

January 2004, 68 pages.

In this thesis, RXTE observations of 4U 1907+09 are presented. Timing analysis of these data sets have yielded quasi periodic oscillations (QPOs) at orbital phases corresponding to the two flares in every orbital period. Known continuous spin down trend and QPO behaviour at the flares strongly suggest that a transient accretion disk occurs at the flares. Our findings strongly suggested that neutron star passes through the equatorial wind of Be companion star. During these passages a transient disk forms around Be neutron star.

Keywords: Accretion powered pulsars, neutron stars, accretion disks, RXTE observations, quasi periodic oscillations.

ÖZ

ROSSI X-RAY TIMING EXPLORER (RXTE) UYDUSUNUN ZAMAN GÖZLEMLERİ

BEKLEN, ELİF
Yüksek Lisans , Fizik Bölümü
Tez Yöneticisi: Prof. Dr. Altan Baykal

Ocak 2004, 68 sayfa.

Bu tezde 4U 1907+09'un RXTE gözlemleri sunulmaktadır. Bu veri setinin zamanlama analizi her bir yörünge periyodundaki iki parlamaya denk gelen yörünge fazlarındaki oldukça yarı periodik salınımları verir. Parlama sırasındaki bu bilinen sürekli yavaşlatıcı eğilim ve yarı periodik salınım davranışı, parlama sırasında geçici bir aktarım diskinin görüldüğünü ve bu çalışma ile bulduklarımız nötron yıldızının Be tipli eş yıldızının ekvatoral rüzgarından geçtiğini önemli bir şekilde önermektedir.

Anahtar Kelimeler: Aktarım güçlü atarcalar, nötron yıldızları, kütle aktarım diskleri, RXTE gözlemleri, yarı periodik salınımlar.

ACKNOWLEDGMENTS

I would like to express my deepest gratitude to Prof. Dr. Altan Baykal for his help, attitude, guidance and insight throughout the research.

My great thanks are due to my mother, father and dear sister for their morale, endless help and encouragement all throughout my life.

I also would like to thank Çağdaş Sıtkı İnam and Özgür Taşkın for their patiences, help during this study.

TABLE OF CONTENTS

ABSTRACT iii

ÖZ iv

ACKNOWLEDGMENTS v

TABLE OF CONTENTS vi

LIST OF TABLES viii

LIST OF FIGURES ix

CHAPTER

1 INTRODUCTION 1

2 THEORY ON ACCRETION POWERED PULSARS 4

2.1 Accretion powered pulsars 4

2.2 High mass accretion X-ray binaries and Low mass accretion X-ray binaries 5

2.2.1 LMXB 6

2.2.2 HMXB 7

2.3 Disk Formation 10

2.3.1 Propeller Mechanism 15

2.4 Spin-up and Spin-down behavior of Pulsars 16

2.5 Quasi-periodic oscillations and the models 19

3 4U 1907+09 27

4 RXTE OBSERVATIONS AND DATA ANALYSIS 35
4.1 RXTE observations 35
4.2 Fourier transform analysis 36
4.3 Determination of confidence level 37
5 DISCUSSION AND CONCLUSION 42
REFERENCES 46
APPENDICES 49
A Light curves and power spectra 49

LIST OF TABLES

TABLE

3.1 Pulse period history of 4U 1907+09 29
3.2 Properties of QPOs in X-ray Pulsars 34
4.1 Journal of observations for 4U 1907+09 35
4.2 Time-period for 4U 1907+09 at 6σ and above confidence level . . 39
4.2 (continued) 40
4.2 (continued) 41

LIST OF FIGURES

FIGURE

2.1 Distribution of accretion powered pulsars in galactic coordinates (Chakrabarty,1996) 6

2.2 Spin period versus orbital period for the accretion powered pulsars with high mass companions 8

2.3 An accretion disk around a magnetic neutron star (Ghosh & Lamb 1979b) 12

3.1 Pulse period history of 4U 1907+09 30

5.1 Frequency versus Orbital Phase for 4σ (upper panel) and 6σ (lower panel) values 44

5.2 Count rate in RXTE-PCA (upper panel) and ASM (lower panel) versus Orbital Phase. 45

A.1 Light curves and power spectra of 10155 50

A.1 (continued) 51

A.1 (continued) 52

A.2 Light curves and power spectra of 10154 53

A.2 (continued) 54

A.2 (continued) 55

A.2 (continued) 56

A.3 Light curves and power spectra of 30093 57

A.3 (continued) 58

A.3 (continued) 59

A.3 (continued) 60

A.4 Light curves and power spectra of 60061 61

A.4 (continued) 62
A.4 (continued) 63
A.4 (continued) 64
A.4 (continued) 65
A.4 (continued) 66
A.4 (continued) 67
A.4 (continued) 68

CHAPTER 1

INTRODUCTION

X-ray pulsars are rotating and strongly magnetized (B$\gtrsim$$10^{12}$G) neutron stars that accrete gas from a stellar companion, either from a stellar wind or by Roche-lobe overflow. Mainly as the accreting material approaches the neutron star, the plasma is channeled to the magnetic polar caps, where it releases its gravitational energy as X-radiation; these rotating hot spots are the source of the pulsed emission. Such emission is beamed and thus produces X-ray pulsation by periodically passing through the line of sight as the neutron star rotates, if the magnetic and rotation axes of the neutron star are misaligned. Neutron stars of this type are called 'Accretion Powered Pulsars'.

Accretion powered X-ray pulsars are classified according to the mass of companion star as either low mass X-ray binaries (LMXBs have late type or degenerate dwarf companion with $M_c < 2.5M$) or high mass X-ray binaries (HMXB) ($M_c > 6M$). HMXB are divided into two subgroups as Be type companion star and the supergiant type. In these X-ray pulsars mass transfer can be seen by either disk-fed or wind-fed. In LMXB, mass transfer occur only if the companion star fills its Roche lobe and the Keplerian disk forms around the neutron star. In HMXBs, with a short orbital period, there is a possibility of accretion via Roche lobe overflow, with a large orbital period, there is a possibilty of accretion via wind because of a seperation in a binary for Roche lobe.

Pulse frequency changes in X-ray pulsars can determine the torque on the pulsars. The torque depend on mainly the magnetic field strength of the neutron star and the geometry of the accretion flow to the star. The accretion torque is the sum of the specific angular momentum of material and the magnetic field lines that interacts with the outer parts of the disk. In particular region of the disk, the total mass captured by the magnetic region act as a spin up or spin down.

4U 1907+09 is an accretion powered X-ray binary pulsar that is accreting plasma from a companion star. The pulsar shows persistent spin down behaviour since 1983 and this slowing down behaviour may be because of the retrograde accretion disk around Be star during the flaring activity. Another characteristic property of 4U 1907+09 is to show QPOs. QPOs are considered to be related to the motion of the accretion disk. Some models are used to explain the QPO trends in X-ray pulsars such as EXO 2030+375, A0535+262, 4U 0115+63, V0332+53, XTE J1858+034, GRO J1744-28, Cen X-3, SMC X-1, X-Per, Her X-1, 4U 1626-67 and almost all models verify the formation of an accretion disk especially during the QPO production.

In this study, we observe the QPO trend of 4U 1907+09 by using data collected with the RXTE PCA instrument. As a result of this analysis we look at the QPOs in 6σ confidence level by using the power spectrum. We expect to see two peaks while the neutron star passes twice through the accretion disk of Be star in every cycle. While passing through the disk, the pulsar shows flaring activity and during that activity the QPOs are occured.

In the next chapter, theory on accretion powered pulsars is presented. The different properties of accretion powered X-ray 4U 1907+09 are reviewed in Chapter 3. In Chapter 4, the frequency values according to the orbital phases are tabled for each observation. In Chapter 5, the flaring activity and the QPO properties of 4U 1907+09 is discussed and lastly the figures of each observation are available in Appendix A.

CHAPTER 2

THEORY ON ACCRETION POWERED PULSARS

2.1 Accretion powered pulsars

The first X-ray source outside the solar system was discovered back in 1962 by (Giacconi et al.1962). This source, Sco X-1, was found to be an accreting binary neutron star. Soon after the discovery of an X-ray pulsar in the Crab Nebula, X-ray pulsations were detected by the Uhuru satellite from two eclipsing X-ray binaries: Centaurus X-3 and Hercules X-1. The discovery of radio and X-ray pulsars provided firm evidence for the existence of the neutron star as a celestial object, which had been predicted theoretically in the 1930's. X-ray astronomy satellites such as Uhuru, Ariel V, SAS 3, HEAO 1, Einstein, Tenma, EXOSAT, Ginga, ROSAT, RXTE, IXAE, XMM, Chandra, and Integral have been used to find new X-ray sources and nearly 217 X-ray pulsars (Guseinov et al. 2000) have been discovered so far.

X-ray pulsars are rotating and strongly magnetized ($B \gtrsim 10^{12}$G) neutron stars that accrete gas from a stellar companion, either from a stellar wind or by Roche-lobe overflow. Mainly as the accreting material approaches the neutron star, the plasma is channeled to the magnetic polar caps, where it releases its gravitational energy as X- radiation; these rotating hot spots are the source of the pulsed emission. Such emission is beamed and thus produces X-ray pulsation by periodically passing through the line of sight as the neutron star rotates, if the magnetic and rotation axes of the neutron star are misaligned. Neutron stars of this type are called 'Accretion Powered Pulsars'. Accreted plasma also carries angular momentum to the neutron star so that the neutron star is exerted torque causing a change in the spin period.

About 48 accretion powered pulsars are known with pulse periods ranging from 0.0031 s to 135.6 min.

Most of these pulsars lie in the galactic plane, a few are located in the magellanic clouds and a few are in the high-latitudes of our galaxy (see Figure 2.1).

2.2 High mass accretion X-ray binaries and Low mass accretion X-ray binaries

Accretion powered X-ray pulsars are classified according to the mass of companion star as either low mass X-ray binaries (LMXBs have late type or degenerate dwarf companion with $M_c < 2.5M$) (Her X-1, GX 1+4, 4U 1626-67, GRO J1744-28 etc.) or high mass X-ray binaries ($M_c > 6M$) (Vela X-1, GX 301-2, OAO 1657-415, SMC X-1, LMC X-4, 4U 1907+09, EXO 2030+375 etc.) High mass X-ray binaries may be divided into two subclasses; (1-i) the short pulse-period systems with very high X-ray luminosity (SMC X-1 with luminosity $6{\times}10^{38} ergs.s^{-1}$, Cen X-3 with $8{\times}10^{37} ergs.s^{-1}$, LMC X-4 with $2{\times}10^{38} ergs.s^{-1}$ and (1-ii) the long pulse-period systems (Vela X-1, GX 301-2, 4U 1538-52, 4U

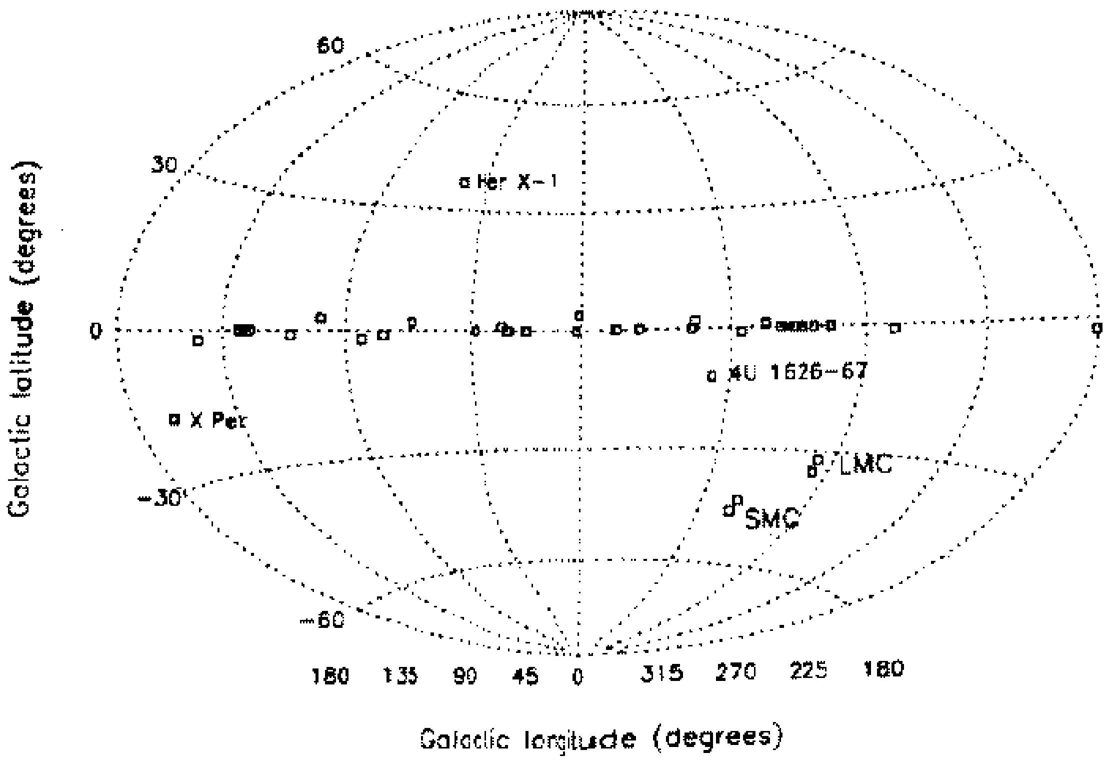

Figure 2.1: Distribution of accretion powered pulsars in galactic coordinates (Chakrabarty,1996)

1907+09, etc.) with moderate X-ray luminosity (Vela X-1 with $6\times10^{36} ergs.s^{-1}$, 4U 1907+09 with $4\times10^{36} ergs.s^{-1}$) (Corbet 1986; Stella et al. 1986).

2.2.1 LMXB

The low-mass X-ray binaries, LMXBs, are steady and low luminosity X-ray sources ($< 10^{37}$ergs s^{-1}). The companion star have a natural wind strong enough to power the X-ray source so significant mass transfer will occur only if the companion fills its critical gravitational potential lobe, the Roche lobe; because of the dominating of X-ray heating of the accretion disk.

2.2.2 HMXB

In high-mass X-ray binaries, were among the first X-ray sources detected and optically identified almost 30 years ago. HMXBs can be further divided into two subgroups (van Paradijs 1983) when the pulse periods are compared with orbital periods: the companion is a Be star (Be/X-ray binary) and a supergiant (SG/X-ray binary). These systems consist of a companion object as; mostly a magnetized neutron star or a black hole. In this kind of binaries: For disk-fed supergiant systems (systems with OB giants) which are quite luminous ($L \gtrsim 10^{37}$ ergs^{-1}), they have short spin periods ($P_{spin} \lesssim 10$ s) and period periods ($P_{orb} \lesssim 4$ days). Short orbital period for such system makes the possibility of accretion via Roche-lobe overflow. So, the Keplerian accretion disk forms around the neutron star and spins-up the neutron star which explains the short spin period. These systems nearly always spin-ups on longer time scales ($> 10^2$ days) (Observations on Cen X-3 have shown a lot of spin up/down behaviours on time scales ($< 10^2$ days) For the wind-fed supergiant systems which has less luminous ($L_x \sim 10^{35}$ - 10^{37} erg s^{-1}), spin ($P > 100$ sec) and orbital periods are larger. Large orbital period makes a seperation in the binary for the Roche-lobe overflow, because of this a stable accretion disk can not be formed. These systems have shown spin up/down transitions on shorter time scales i.e.less than 10 days (Vela X-1, OAO 1657-415).

For the HMXBs, we can roughly estimate type of the system by plotting spin period versus orbital period (see Figure 2.2). This figure is also known as Corbet

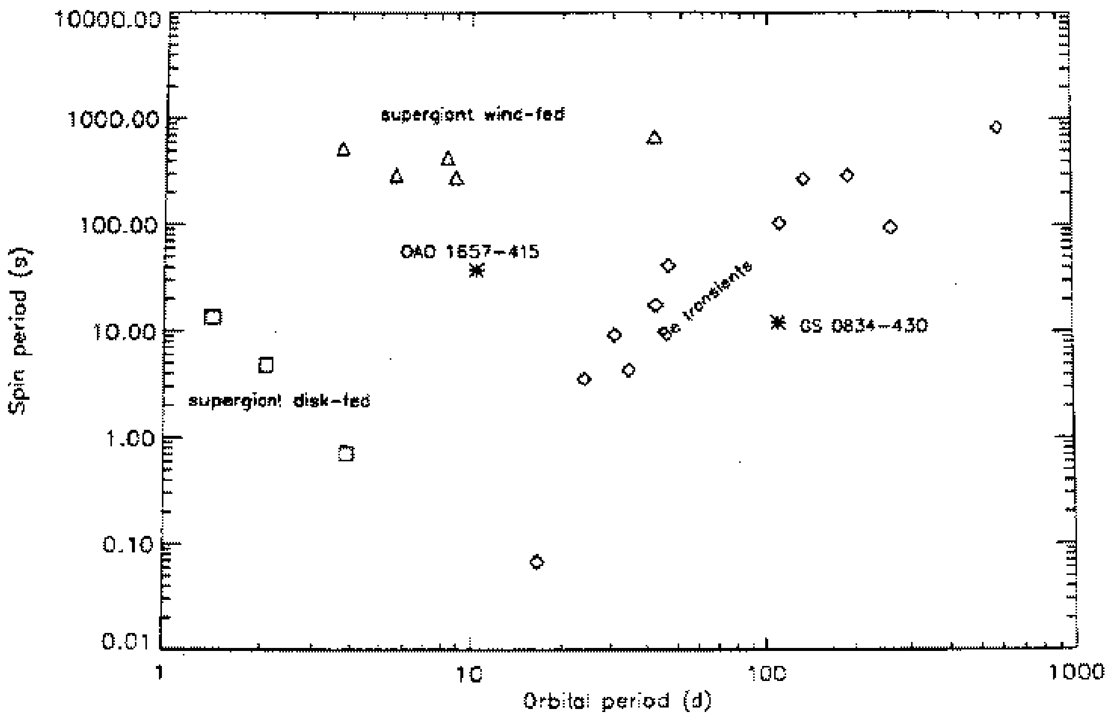

Figure 2.2: Spin period versus orbital period for the accretion powered pulsars with high mass companions

diagram (Corbet 1986; Waters & van Kerkwijk 1989). In this figure, the pulsars are catogarized according to their companion star type. Asteriks are supergiant companions that are Roche lobe filling, squares are supergiant companions that underfill their Roche lobe, circles are confirmed Be-transient binaries and plus signs are those with low-mass ($\lesssim 10\ M_{\odot}$) companions (Her X-1, GRO J1744-28 and 4U 1626-67). Triangles refer to the sources such as; GS 0834-430, OAO 1657-415, GRO J1750-27, 2S 1553-54 and GRO J2058+42.

The majority of the known high mass X-ray binaries are Be X-ray systems (4U 0115+63, A0535+26, GX 304-1 etc.). The systems with Be-star companions are powered by mass accretion through stellar wind capture (called 'wind-fed' pulsars). Most Be systems have relatively wide orbits with moderate eccentricity and their compact companions spend most of their time far away from the disc surrounding the Be stars (van den Heuvel & Rappaport 1987; Bhattacharya & van den Heuvel 1991; Apparao 1994). Be systems are generally observed during transient outbursts which correlated with spin ups in their pulse frequencies. These systems are very often bright pulsating transient sources. X-ray outbursts will be expected during the time of the neutron star‘s periastron passage, from a low-velocity and high-density wind around Be stars. X-ray outbursts from the Be transients can be divided into two types: ’normal’ and ’giant’ (Motch et al. 1991) or equivalently Class I and Class II (Stella et al. 1986). The ’giant’ outbursts are bright and substantial spin-up of the pulsar occurs. In contrast, the ’normal’ outbursts are much fainter (peak flux $< 20\%$ of giant outburst peak) while the pulsar either shows little or no spin-up (or exhibits spin-down) (Scott et al. 1997). Some of the X-ray pulsars, especially those in Be-star X-ray binaries, are of transient nature and many of them appear on a timescale of a few days, and then decay over many tens hundreds of days, some of these have been recured on a timescale that ranges from days to tens of years. They are important in the study of X-ray binaries because of covering the large range in luminosity (typically $10^{34} - 10^{35}$). The transient episodes may result from an instability in the accretion disk, or a mass ejection episode from the companion. There are also Be X-ray binaries that are persistent sources (RXJ0812-311, RXJ0440+443, RXJ1037-564 (known as also 4U 1036-56), RXJ1826-145, RXJ0146+612 etc.).

2.3 Disk Formation

In X-ray pulsars powered by accretion, two types of mass transfer can be seen; disk-fed and wind-fed. In the wind-fed systems, the massive type companion is inside the Roche lobe but loses mass via a stellar wind. Strong stellar winds are driven from the hot atmosphere of companion star by the radiation pressure on the highly ionized atoms. Some of the fraction ($< 0.1\%$) of this wind is captured by the neutron star due to its strong gravitational field and a bow shaped shock front is formed around it. The captured matter has some angular momentum respect to the compact star. In a medium with sound velocity (c_s), a neutron star will capture matter from a fairly cylindrical volume with radius r_a (capture radius)

$$r_a = \left(\frac{2GM}{{\nu_{rel}}^2 + {c_s}^2}\right) \tag{2.1}$$

(A neutron star moves with a relative velocity ${\nu_{rel}}^2 = {\nu_w}^2 + {\nu_{orb}}^2$ and ν_w is the wind velocity at the neutron star orbit.

The captured matter via a stellar wind interacts with the strong magnetic field of the neutron star. The accreting matter is halted by the magnetic pressure at the radius, r_m, where the pressure of falling matter balances the magnetic pressure and the matter is forced to corotate with the neutron star and this accreting matter enforces a closed magnetosphere which means all field lines close themselves within this radius around the neutron star (Arons and Lea 1976a, b, 1980).

$$r_m = 1.9 \times 10^8 \left(L_{37}\right)^{-2/7} \left(\frac{M}{1.4 M_\odot}\right)^{1/7} \left(B_{12}\right)^{4/7} \left(R_6\right)^{10/7} \mathrm{cm}. \tag{2.2}$$

where L_{37} is bolometric X-ray luminosity in units of 10_{37} erg s^{-1}, B_{12} is B in units of 10_{12} gauss and R_6 is R in units of 10_6 cm. Far from the neutron star, the magnetic field has little influence on the flow and the flow is spherically symmetric. When we get close to the stellar surface the field controls the plasma completely and we expect that the field will begin to dominate the flow when the magnetic energy density becomes comparable to the kinetic energy density of the accreting gas. This condition specifies the characteristic radius of the magnetospheric boundary, r_A, called Alfv'en radius. From:

$$
\begin{aligned}
r_m &= (Constant) r_A \\
r_A &= \left(\frac{\mu^4}{2GM\dot{M}}\right)^{1/7} \\
&= 3.5 \times 10^8 {L_{37}}^{-2/7} {\mu_{30}}^{4/7} \left(\frac{M}{M_\odot}\right)^{1/7} {R_6}^{-2/7} \qquad (2.3)
\end{aligned}
$$

where $\dot{M} = LR/GM$ The magnetic field does not penetrate the plasma much beyond r_A. The magnetic field has an influence on the currents in the infalling plasma near the Alfv'en radius.

When the co-rotating companion star has expanded and begins to overflow its Roche lobe, the gas flowing through the inner Lagrange point L_1 possesses significant angular momentum. Some of this matter is captured by the compact star and flows toward it in an accretion disk. This accretion disk can be seen in detail in Figure 2.3. In wind fed systems, the angular momentum may sometimes be sufficient form an accretion disk. The formation of a disk is expected only when the radius of a circular Keplerian orbit r_k of accreted matter with specific

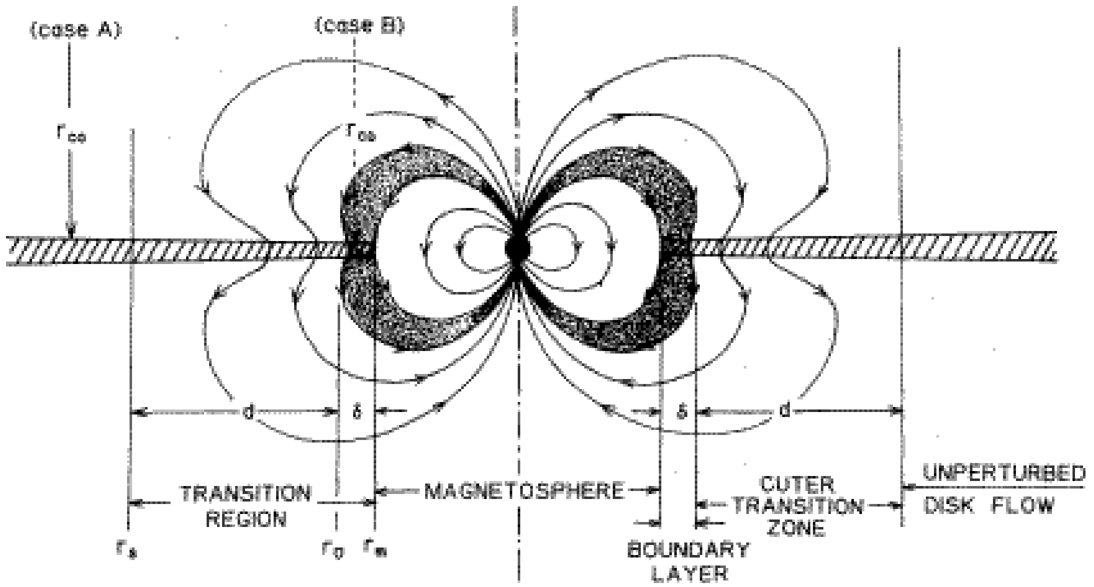

Figure 2.3: An accretion disk around a magnetic neutron star (Ghosh & Lamb 1979b)

angular momentum l is larger than the r_m:

$$r_k = \left(\frac{l^2}{GM}\right) > r_m$$

Accretion will be inhibited by a centrifugal barrier if the pulsar magnetosphere rotates faster than the Keplerian frequency at the inner disk boundary and for occuring of accretion the magnetospheric radius should be inside the corotation radius (r_{co}) which means $r_{co}>r_m$. It is derived by equating rotational velocity to the corotating Keplarian velocity:

$$\begin{aligned} \omega r_{co} &= \left(\frac{GM}{r_{co}}\right)^{1/2} \\ r_{co} &= \left(\frac{GM}{\omega^2}\right)^{1/3} \\ r_{co} &= 2.8 \times 10^8 P^{2/3} \left(\frac{M}{1.4 M_\odot}\right)^{1/3} \text{ cm} \end{aligned} \tag{2.4}$$

where P is the spin period of the neutron star.

The magnetospheric boundary at the magnetic equator occurs approximately at a radial distance r_o:

$$\begin{aligned} r_o &= [1/2v_{in}(r)v_{ff}(r)]^{2/7}\,\mu^{4/7}\,(2GM)^{-1/7}\,\dot{M}^{-2/7} \\ &\simeq 5.2\times10^{8}\mu_{30}{}^{4/7}\dot{M}_{16}{}^{-2/7}M/M_{\odot}{}^{-1/7}\mathrm{cm} \end{aligned} \quad (2.5)$$

for spherical accretion (Davidson and Ostriker 1973; Lamb et al. 1973) where μ is magnetic moment in units of Gauss cm^3 and μ_{30} is μ in units of 10^{30} Gauss cm^3.

$$\nu_{in}\,(\simeq 0.1v_{ff})$$

$$\nu_{ff} = [(2GM/r)]^{1/2}$$

where ν_{in} is the infall velocity of matter and v_{ff} is free-fall velocity.

When we look at the internal parts of Figure 2.3, we see that magnetic field lines behave differently in each part. Between the radius r_a and r_s, the effect of the magnetic field of the neutron star the magnetic pressure. There is also magnetic field lines extending over the r_s (screening radius) and threads as a part in the accretion disk. Between r_s and r_o, the angular velocity of the accreted matter starts to decrease to the angular velocity of the neutron star. In this region magnetic field lines begin to thread the disk without distrupting the disk completely, it is called 'Outer Transition Region'. In the 'Case A' (Figure 2.3), if $r_o<r_a$ and $r_o<r_{co}$, the matter captured from the wind flows from the r_a to the r_m. The matter halted at the magnetopause gets onto the field line sand goes into r_m along the dipole magnetic field lines. In the 'Case B', if $r_{co}<r_o<r_a$, the

wind matter is stopped at the magnetospheric boundary and cannot penetrate any more. Thus the material may be ejected beyond the r_a via the 'propeller' mechanism. In the region between r_o and r_A, the magnetic field lines force the plasma to rotate with the neutron star's angular velocity. The width is small compared to r_A. And, between r_A and R (radius of the star), no disk formation is occured and the matter accretes to the star by means of the magnetic field lines.

If the accreted matter has enough angular momentum then a disk can be formed in the wind-fed pulsars and the interaction between a stellar wind and an axisymmetric accretion flow onto a star will lead to the formation of a shock front as a bow-shaped shock. This accretion disk is expected to be formed near the neutron star behind the shock front of the stellar wind, but this disk is unstable and may change its configuration as large fluctuations of accretion torque on the neutron star. In wind-fed pulsars, for Be type star: Corbet (1984, 1986) suggested that the pulse periods of the neutron star in Be systems are correlated with the orbital periods and the periastron distance of the systems. In these type systems X-ray outbursts are considered to occur when a neutron star in an eccentric orbit passes near periastron through a circumstellar envelope around Be star and Shibazaki et al.(1982) considered an inclined orbit of the neutron star with respect to a disk-like or a shell-like wind or a ring of matter emanating from the Be star. These indicate that the neutron star in such systems is in a quasi-equilibrium state in which r_{co} and r_m are about equal. When the neutron star passes through this disk near periastron, $\dot{M}$ increases and the inner edge of the disk is pushed inward so the rapid spin up occurs during outbursts but when the neutron star moves away from periastron in the eccentric orbit, $\dot{M}$ decreases and almost ceases. During this phase the disk shrinks away with the inner radius exceeds back to about the r_{co} or farther. Once the r_m exceeds r_{co} when the star is far from periastron, then the accreted matter cannot penetrate the magnetosphere and is 'propelled' away.

2.3.1 Propeller Mechanism

The 'propeller' mechanism that take place when pulsar magnetosphere grows beyond the co-rotation radius as a result of the decrease in mass accretion rate and the centrifugal force prevents accreting matter from reaching the magnetic poles. When the mass accretion rate increases, the magnetosphere is usually small compared to the corotation radius at which the angular veloctiy of Keplerian motion is equal to the angular velocity of the neutron star. Material is continuously channeled to the magnetic poles and 'hot spots' pulsate. When the accretion rate decreases, the magnetosphere expands. As it grows beyond the corotaion radius, the centrifugal force prevents material from entering the magnetosphere and accretion onto poles can not be seen so no X-ray pulsation is expected such as in GX 1+4 and GRO J1744-28 (Cui 1997), so in order to keep the propeller effect from preventing accretion onto the neutron star and we need $r_{co}>r_m$ condition.

2.4 Spin-up and Spin-down behavior of Pulsars

From long term monitoring of the pulse periods of X-ray pulsars, we can express the behavior of the accretion powered X-ray pulsars as: 1. Spin-up: a linear decrease with time in the pulse period; when a neutron star spin-ups, its period will decrease because of the angular momentum gained from the accretion flow (Pringle and Rees 1972; Davidson and Ostriker 1973; Lamb et al. 1973), 2. Equilibrium state: only a random walk in the period, 3. Spin-down: a steady increase in period.

From the observations of pulse frequency changes in X-ray pulsars, the signs of the torque exerted on the pulsars can be determined by these changes. The torque depend on mainly the magnetic field strength of the neutron star and the geometry of the accretion flow to the star. The accretion torque is the sum of the specific angular momentum of material and the magnetic field lines that interacts with the outer parts of the disk. The torque from the angular momentum of material always make the star to show spin up behaviour, rotating in the same direction with the disk flow and the torque from the magnetic field lines threading the disk outside r_{co} make it to show spin down behaviour. According to standard model of an accretion disk (Ghosh and Lamb 1979), if $r_s<r_{co}$ (in Case A)(see Figure 2.3), the total mass captured by the magnetic field in the region $r_m<r<r_s$ act as a spin-up torque. On the other hand if $r_s>r_{co}$, the magnetic field lines outside r_{co} also thread the disk in the region $r_{co}<r<r_s$, thus contributed as a spin-down torque. Only the matter captured by the magnetic field lines in the

region $r_m<r<r_{co}$ tranfers spin-up torque. According to this model both spin-up and spin-down torque is possible.

If the accretion is from a Keplerian disk at the inner disk edge, the magnetosphere disturbs the Keplerian rotation of the disk, forcing matter to accrete along magnetic field lines. This inner edge of the disk r_o (see Equation 2.5) gets smaller as the mass accretion rate increases. In early observations it is believed that most accreting pulsars were spinning up according to below equation.

$$N = \dot{M}\left(GMr_m\right)^{1/2} \tag{2.6}$$

where N is an accretion torque. This was strong evidence that X-ray pulsars must be compact stars with large magnetospheric radii. But Her X-1 and Cen X-3 pulsars were found to be spinning up much more slowly than Equation 2.6. Furthermore, these pulsars sometimes show short spin-down behaviour. In some systems, a star capturing material from a disk with the same rotation actually lose angular momentum while continuing to accrete. It can be explained as the spin-up accretion torque must decrease eventually become negative. This is called an equilibrium state and most of the X-ray pulsars should have reached this equilibrium state (Ghosh & Lamb 1979). In this equlibrium state, magnetic field lines that thread the disk beyond the r_{co} where the disk rotates more slowly than the star, are swept back and transport the angular momentum outward and a negative torque is exerted on the neutron star. When the neutron star close to equilibrium it will be spun down, even though accretion continues. So stars close to equilibrium will spin up much more slowly than Equation 2.6 and show spin down bahviour while continuing to accrete. According to standard accretion torque, Equation 2.6 can be rewritten as:

$$\begin{aligned} N &= n(w_s)\dot{M}\,(GMr_o)^{1/2} \\ N &= 2\pi I \mid \dot{\nu} \mid \end{aligned} \tag{2.7}$$

where I is the neutron-star moment of inertia ($\simeq 10^{45}$gcm^2) and $\dot{\nu}$ is the rate of change of the frequency. $n(w_s)$ is a dimensionless torque measuring the variation of the accretion torque and w_s is a fastness parameter.

$$\begin{aligned} w_s &= \nu/\nu_k = r_o/{r_{co}}^{3/2} = 2\pi^2\dot{\nu}\mu^{6/7}(GM)^{-5/7}\dot{M}^{-3/7} \\ n(w_s) &\sim 1.4(1 - w_s/w_c)/(1 - w_s) \end{aligned} \tag{2.8}$$

One of the important parameter to determine the behaviour of the star is critical parameter (w_c)(Ghosh & Lamb (1979a)) at which the accretion torque is expected to vanish. The critical value depends on the azimuthal pitch of the magnetic field lines in the boundary layer near the Alfv'en radius and $w_c \sim 0.35$. The torque will spin up if the neutron star is rotating slowly ($w_s < w_c$) in the same direction with the disk flow, but it will spin down if it is rotating rapidly ($w_s > w_c$). However, accroding to the observations in some pulsars like 4U1627-67, Cen X-3 the torque behaviour does not obey to this rule (Shinoda et al. 1990 and Takeshima et al. 1991).

For example in GX 1+4 the spin down behaviour is resulted from a retrograde accretion disk (Nelson et.1997). A retrograde accretion disk is opposite the correlation expected from the standard theory assuming the torque is correlated with the observed. In standard theory there is a positive correlation between changes in pulse frequency derivatives and the X-ray luminosity (or mass accretion rate). If this pulsar is accreting from a retrograde disk, the material really carries negative angular momentum relative to the neutron star rotation. As long as the magnetosphere is far inside the corotation radius ($r_{co} \gg r_m$), a reversed disk should produce a spin-down torque of similar magnitude to the spin-up torque from a prograde disk. In fact it is not easy to form a retrograde accretion disk in the case of accretion via Roche lobe overflow, mostly the prograde and the retrograde disk forms in wind-fed systems.

2.5 Quasi-periodic oscillations and the models

One of the useful result to studying the accretion disk around the accretion-powered X-ray binaries are the (QPOs) that have been considered to be related to the motion of the accretion disk especially the innerparts. QPOs with frequencies in the 5-220 mHz range have been observed from X-ray pulsars (Monn and Eikenberry, 2001) (Boroson et al. 2000 and references therein). There are various models described to explain the QPOs. Mainly, these can be defined as: 1.Accretion flow instabilities, 2.Keplarian-frequency model, 3.The beat-frequency model (involving Keplarian motion and neutron star rotation).

Accretion flow instabilities, this model has been proposed for the 6 Hz normal-branch QPO in z-type sources (Hasinger and van der Klis, 1989) and implies an X-ray luminosity close to the Eddington limit. To get the Eddington limit, suppose that a relativistic object which has R_x radius at a surface at which the whole kinetic energy is transformed into radiation. Because, a neutron star which has a solid surface and a magnetic field mainly radiates as a result of collisions. The matter falls freely so that a unit mass has a kinetic energy GM/R. If the amount of substance falling per unit time on the surface is $M\dot{g}$. The total luminosity of the accreting star is given by

$$L = \frac{GM\dot{M}}{R} \tag{2.9}$$

Let σ be the cross section of interaction of the emitted radiation with matter. The force acting on the incident particles is $\sigma\ L/(4\pi R^2 c)$. It depends on the distance as in the gravitational force GMM_p/R^2 (for a particle on the surface). For a certain value of the luminosity $L = L_{Ed}$ called Eddington limit, these forces become equal:

$$L_{Ed} = \frac{4\pi GMm_p c}{\sigma} \tag{2.10}$$

In the case of Thomson scattering, σ=σ_T and $\sigma_T/m_p \approx 0.4\mathrm{cm}^2/\mathrm{g}$ (for hydrogen); this gives such an estimate to get the general form of the 'Eddington limit':

$$L_{Ed} \approx 1.3 \times 10^{38} \frac{M}{M_\odot} \mathrm{ergs}^{-1} \tag{2.11}$$

The luminosity of any source, cannot exceed this 'limit' for steady state when there is a spherically symmetric accretion onto a neutron star. Because, the pressure of the emergent radiation at this 'limit' luminosity balances the gravitational pressure of the accreting matter. If there is any increase in luminosity above this 'limit' value, the accretion will stop.

Z sources are thought to be X-ray binaries containing low magnetic field neutron stars (Sco X-1, GX 5-1, GX 349+2, GX 17+2, GX 340+0). Z sources produce Z-shaped patterns in X-ray CDs (colour-colour diagrams) and HIDs (hardness versus intensity diagrams). There are 3 branches in Z shape; horizontal branches, normal branches and flaring branches. Normal branch QPOs have frequencies between 4.5 and 7.0 Hz and amplitudes between 1-10 keV band, and they are strongest near the middle of the normal branch.

Keplerian-frequency model (KFM), in this model the QPOs are produced as a result of the absorption of X-rays by inhomogeneities in the inner edge of the Keplerian disk which attenuate the pulsar beam regularly. The QPO center frequency is given by the Keplerian frequency at the inner edge of the accretion disk.

$$\nu_{(QPO)} = \nu_{(K)} \tag{2.12}$$

The QPO frequency in this model is given by the Keplerian frequency at r_m,

$$\nu_K(r_m) = (1.1Hz)M^{2/7}{R_6}^{3/7}{\mu_{30}}^{-6/7}{L_{37}}^{3/7} \tag{2.13}$$

where R_6 is R(radius of the neutron star) in units of 10^6 cm, L_{37} is luminosity in units of 10^{37} ergs^{-1},μ_{30} is ν in units of 10^{30} gauss cm^3. In the KFM,

$$\nu_{(spin)} < \nu_{(QPO)} = \nu_{(K)}$$

this condition should be observed otherwise the accretion could be prohibited by 'propeller effect'.

Beat-frequency model (BFM), in this model (the QPOs are produced when the material infall onto the pulsar from the accretion disk is modulated at the

Keplerian frequency) QPOs originate from the inhomogeneity of the accreting matter at the inner edge of the accretion disk; so, the QPO frequency is the difference between the frequency of the neutron star rotation and that of the accreting disk matter at the magnetospheric boundary assumed to be in Keplerian motion near the corotation radius.

$$\begin{aligned} \nu_{QPO} &= \nu_K - \nu_{spin} \quad (2.14) \\ \nu_K &= \nu_{QPO} + \nu_{spin} \end{aligned}$$

Acording to BFM, r_m from the standard accretion disk theory which is explained in Equation 2.2 is consistent with the r_m by assuming the BFM.

$$r_m = \left(\frac{GM}{4\pi^2\nu_K}\right) \quad (2.15)$$

M is the mass of the neutron star. Mainly we can say that BFM explains QPOs as luminosity oscillations, the KFM explains QPOs as beaming oscillations. To understand the QPOs in more details, it is important to look at QPOs observed in different sources. Here there are some examples in which QPOs have been detected (Paul and Rao 1998). The transient X-ray pulsar; the high mass X-ray binaries (HMXRB) EXO 2030+375 (Angelini et al. 1989), A0535+262 (Finger et al. 1996), 4U0115+63 (Soong & Swank 1989), and V0332+53 (Takeshima et.al 1994), 4U1907+09 (in't Zand et al. 1998, Mukerjee et.al 2001), XTE J1858+034 (Paul & Rao 1998) and the LMXB GRO J1744-28 (Zhang et al. 1996). In some of the persistent HMXRB sources: Cen X-3 (Takeshima et al.1991), SMC X-1 (Angelini et al. 1991), X-Per (Takeshima 1997), Her X-1 (Boroson et al. 2000) and the LMXRB 4U1626-67 (Shinoda et al. 1990; Kommers et al.1998). We can look at these pulsars according to the QPO models which comply with the observations and their origins: Both the Keplerian frequency model and the beat frequency model are ideal models for the pulsars EXO 2030+375, A0535+262, XTE J1858+034, LMC X-4, since these models comply with the observations of these pulsars.

In EXO 2030+375, QPOs were detected during an outburst when the source was very close to its maximum observed luminosity. Since this pulsar has a large spin-up and as a result of this; the accretion disk penetrates inside the corotation radius, the QPOs models involving the interaction between the magnetosphere of a rotating neutron star and an accretion disk. Since the magnetosphere prevents the formation of an accretion disk close to the neutron star, the QPOs may not result from the instabilities at the boundary between an accretion disk and the neutron star surface (Angelini et al. 1989).

In XTE J1858+034, the observed low frequency of the QPOs should indicate a large magnetosphere, in which the $r_m \simeq 7.2 \times 10^8$cm, so the QPOs are originated from either inhomogeneities in the Keplerian disk at the magnetospheric boundary which attenuate the pulsar beam regularly at its rotation frequency, or the material influx to the pulsar from the disk which modulated at the Keplarian frequency. The QPOs are found to be stronger at higher energy which favours the beat frequency model (Paul and Rao 1998).

In LMC X-4 pulsar, since the mHz QPOs only appear during the large X-ray flares, the aperiodic variabilities can be classified as 'big QPOs (BQPOs)' and 'medium QPOs (MQPOs)'. BQPOs can be expressed by the beating between the pulse frequency of the neutron star and the Keplerian frequency of large accreting clumps near the corotation radius; so these BQPOs originate near the corotation radius. MQPOs can be expressed as; the observed frequencies represent the Keplerian orbital frequencies of clumps and these MQPOs originate from the orbital motions of clumps in the accretion disk outside the corotation disk. Lastly, the increase of the highest QPO frequencies in this pulsar may be for the evidence of an infalling motion of the accretion disk inner edge as the flares continue (Moon and Eikenberry, 2001).

The Keplerian frequency model is not appropriate model for the pulsars 4U 0115+63, Cen X-3, 4U 1626-67 and SMC X-1. Since the observed QPO frequencies are founded to be lower than the pulsation frequency. (As we know if the Keplerian frequency at the magnetospheric boundary is less than the spin frequency, the centrifugal inhibition of mass accretion will be seen).

In Cen X-3, when the QPO is analyzed, it was understood that the QPOs are not produced by partial occultations of the emission region but generated by modulating the mass accretion rate onto neutron star polar caps. The fastness parameter of this pulsar is 0.855. Even this value is much larger than $w_c (w_c \sim 0.35)$, a spin-up behavior is expected. From the observations, the pulsar has also shown spin-up behavior. This result is similar to that for 4U 1626-67 (Takeshima et al. 1991).

In 4U 1626-67, while the magnetic dipole moment is calculated theoretically from accretion disk model, the v_K is used by the BFM. This μ_{30} consistent with an estimate on the shape of the hard X-ray spectrum of this pulsar. The ν_{QPO} is consistent with the beat frequency between the ν_{spin} and $\nu_K(r_a)$ (Shinoda et al. 1990).

In SMC X-1, the QPOs may arise from the interaction of the innermost region of the accretion disk with the rotating neutron star magnetosphere. When it is compared, the r_A value of Ghosh and Lamb (1979a,b) is nearly equal to the r_A value according to the BFM (Angelini et al.1991).

Both the Keplerian and the beat frequency model may also be inapplicable for the HMXRB V0332+52 (The magnetospheric boundary calculated from the QPO and the observed luminosity does not relate with this source) and LMXRB GRO J1744-28 pulsars.

In GRO J1744-28, the observed QPOs are different from these classical QPO models seen among Z sources and X-ray pulsars. The QPOs of this pulsar can be expressed as neutron star g-mode oscillations and photon bubble oscillations. Shortly, the time variability of the X-ray flux results mainly from the interaction of radiation and the accreted matter, as a result this variability produces a photon bubble instability resulting in bubble oscillations at specific frequencies (Zhang et al. 1996).

In Her X-1, two kinds of QPOs were observed. These do not arise in the accretion disk, they arise on the X-ray heated face of the companion star (HZ Herculis). These QPOs are due to material that absorbs the X-ray and prevents them from heating HZ Her rather than material that emits X-ray. It can be said that the higher frequency QPO results from a global vertical oscillation of the disk and the lower frequency QPO results from Keplerian rotation (Boronson et al.2000).

In the LMXBs EXO 0748-676 and 4U1915-05 showing dipping activity, kHz QPOs are observed. The QPOs are mostly caused by an orbiting structure in the accretion disk, which modulates the radiation of the central source.

CHAPTER 3

4U 1907+09

4U 1907+09 is an accretion-powered X-ray binary pulsar that is accreting plasma from a companion star. The X-ray observations of flaring activity in 4U 1907+09 at regular intervals during each of its orbital cycles suggests that its companion is likely to be a Be star (Marshall & Ricketts, 1980; Makishima et al. 1984; Cook & Page, 1987). The observed X-ray flares with a difference in phase of 0.45 orbital period may result from the pulsar intersecting the extended disk of the Be star twice in each orbital cycle. The optical observations of Iye (1986) shows variable H_α emission with large equivalent width, which is an important characteristics of Be star. Similar variations have also been observed in another X-ray binary pulsar with a Be companion, V0331+53. But, the relationship between the spin and orbital periods in the Be binary pulsars given by Corbet (1984) does not hold in the case of 4U 1907+09. So the companion should be discussed according to other 'companion type'. Firstly, according to Corbet diagram, it is positioned as OB supergiant. Also, the other characteristics of Be systems such as longer duration giant outburst activities, as seen in the case of A0535+26 and high eccentricity are not observed in our pulsars. The observations of the wind-fed X-ray pulsar GX 301-2, having an OB supergiant companion, show two flares per orbit as in the case of 4U 1907+09. These arguments show that the companion star in 4U 1907+09 pulsar can be either a Be star or an OB supergiant.

The source was discovered as an X-ray source and it has been observed from various X-ray observatories since its discoverey in the Uhuru survey by Giacconi et al. (1971) and instruments on board Ariel V (Marshall & Ricketts, 1980), Tenma (Makishima & Mihara, 1992; Mihara 1995), RXTE (in‘t Zand, Baykal & Strohmayer, 1998a; in‘t Zand, Strohmayer & Baykal, 1997, and 1998b), BeppoSAX and IXAE (Mukerjee et al. 2001).

The orbital period of 4U 1907+09 is firstly determined as 8.38 days through an analysis of data taken over course of 5 yr from an instrument on Ariel V (Marshall & Ricketts, 1980).

The pulse periods measured with X-ray satellites have been presented in Table 3.1 and Figure 3.1. The quoted uncertainty in the pulse period corresponds to a 1 σ confidence level. The period derivatives were calculated with respect to the Tenma observations in 1983 August. The spin-down rate of 4U 1907+09 measured from IXAE, Tenma observations is nearly 0.23 ± 0.01 syr^{-1}, indicating that the pulsar has been in continuous spin-down since its discovery in 1983. Also the timing measurements carried out by EXOSAT (Cook & Page 1987), RXTE showed continuous spin-down of the neutron star as can be seen from Table 3.1.

As it is maintained, 4U 1907+09 some pulsars show continuous spin-down behavior. It is considered to be mainly two reasons for these continuous spin-downs: 1. Inhibition of accretion disk, 2. Formation of a transient accretion disk

Table 3.1: Pulse period history of 4U 1907+09

Observation	Satellite	MJD	Spin period s	Derivative	Ref.
1983 Aug/Sep	Tenma	45576	437.483±0.004	...	1
1984 May/June	EXOSAT	45850	437.649±0.019	0.221±0.026	2
1990 Sep	Ginga	48156.6	439.19±0.02	0.241±0.003	3
1996 Feb	RXTE	50134	440.341±0.014	0.229±0.005	4
1996 Aug	IXAE	50302.6[a]	440.53±0.01	0.2343±0.0008	5
1996 Dec	RXTE	50440.4	440.4877±0.0085	0.2253±0.0009	6
1998 June	IXAE	50665[a]	440.95±0.01	0.2348±0.0007	5
1998 June	RXTE	51021.9	440.7045±0.0032	0.2035±0.0004	6
1998 Aug	RXTE	51080.9	440.7598±0.0010	0.2185±0.0003	6

[a] Average of MJD for the IXAE observations is given.
REFERENCES - (1) Makishima et el. 1984, (2) Cook & Page 1987, (3) Mihara 1995, (4) in't Zand et al. 1998, (5) Mukerjee et al. 2001, (6) Baykal et al. 2001.

around the neutron star.

The slowing down behavior of pulsars could be due to a lower accretion rate and the resulting centrifugal inhibition of accretion (or the propeller effect). The infalling material is flung away by the carrying part of the rotational energy extracted from the neutron star so this results as slowing down in the neutron star. This slowing down behavior occurs when magnetospheric radius r_m extends closer to the corotation radius which mean to low accretion rates. r_{co} (Ghosh & Lamb 1979a, 1979b; Wang 1987, 1995; Anzer & Borner 1980; Lovelace, Romanova, & Bisnovatyi-Kogan 1995). To look at whether this condition is supplied for 4U 1907+09 or not, the corotation radius (r_{co}) from Equation 2.4 for 4U 1907+09 is nearly 9.6×10^9 cm and (r_m) from Equation 2.2 is nearly 4.1×10^8 cm. Because of $(r_{co}) \gg (r_m)$, in this pulsar lower accretion rate can not be occur and for this pulsar the (r_m) is hard to bring out to such a large corotation radius.

If the 'propeller effect' takes place in most of the binary orbits, this may lead

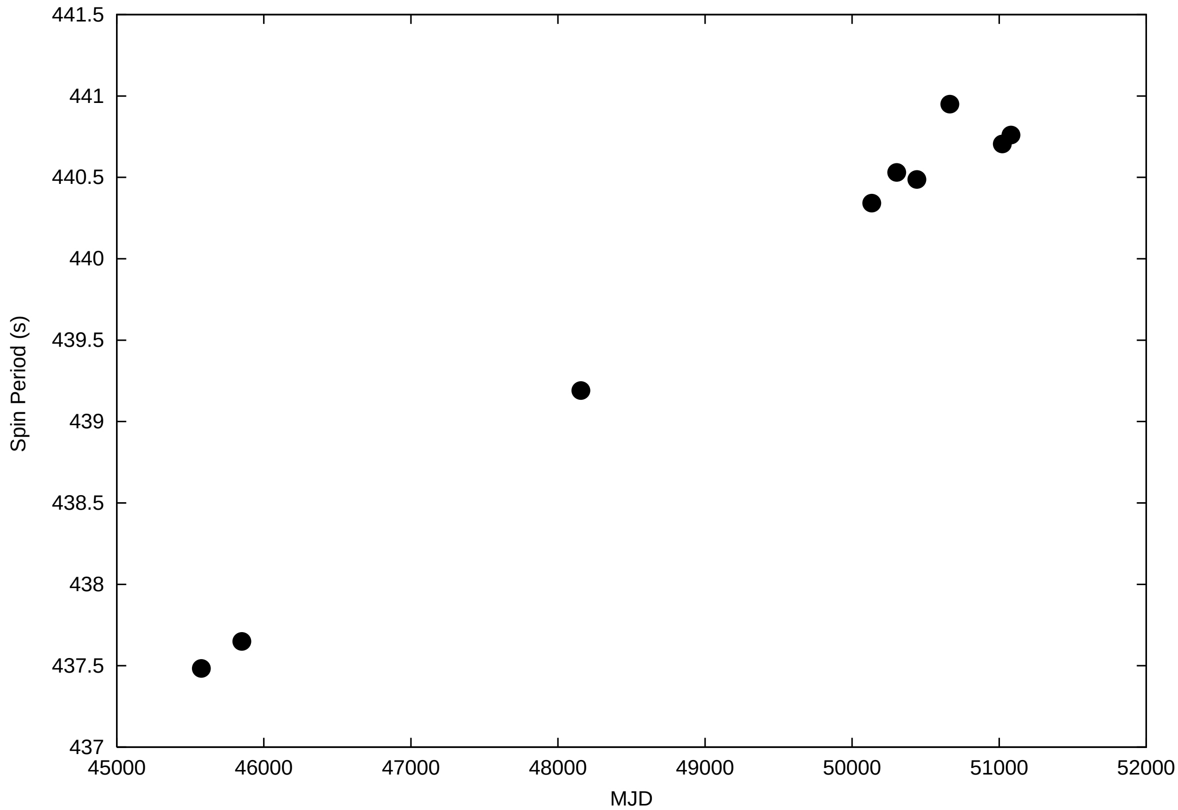

Figure 3.1: Pulse period history of 4U 1907+09

to the observed monotonous spin-down in the pulsar. To look at this effect in 4U 1907+09, begin with the first parameter; the minimum luminosity $L_X(min)$ which an X-ray pulsar begins to slowing down due to centrifugal inhibition of accretion (or for the propeller effect) shall be derived from r_m=r_{co}:

$$L = 2 \times 10^{37} (R_6)^{-1} (M/1.4M_{\odot})^{-2/3} (\mu_{30})^2 (P_s)^{-7/3} \mathrm{erg.s}^1 \quad (3.1)$$

where P_s is the rotation(spin) period.

For this pulsar, this L_x value corresponds to 6×10^{31} erg.s^{-1} (From Equation 3.1, with a mass $1.4M_{\odot}$). This luminosity value is below the L_x value of the IXAE observation. But, according to the RXTE observation, there have been some intermittent declines in the X-ray intensity which is below this L_x during the orbit called 'dipping activity'. These 'activities' covers % 20 of the observation time. Also, these luminosities' count rates are below the background rates of the detectors, it is impossible to observe these 'intermittent propeller effects'. As an example;in one of a Be transient source, GRO J1008-57, although there was declination in the source luminosity about a factor of 100 from the peak, the propeller effect didnot take place.

As we said previously, the QPOs reveal the presence of a transient accretion disk around the flare. And the presence of a transient accretion disk around the neutron star during the flare may be an another explanation for the continuous slowing down of the pulsar. For observing QPO from IXAE data, the accretion disk can be formed close enough to the magnetosphere. Formation such a disk also supports that r_m is substantialy smaller than r_{co}.

A transient disk can provide an alternative explanation to the observed spin-down if this disk is rotating in an opposite direction of the pulsar spin, because formation of such a disk may supply the necessary torque to the neutron star to explain the spin-down rate. The sufficient torque of the duration which causes the slowing down of the pulsar can be found by equating the torque definitions in Equation 2.7. To provide enough negative torque on pulsar, the duty cycle of the neutron star lasts on the order of a few percent of the binary period. When we equate these torques, the η is found to be 0.029 from 1996 February RXTE (in't Zand et al. 1998) and 0.024 from 1996 August IXAE (Mukerjee et al.2001). This corresponds to a duration of nearly 0.24 days for the binary period of 8.38 days.

Therefore, a retrograde accretion disk of the above estimated duration during the flare could supply negative torque to explain the observed spin-down of the pulsar.

Lastly, here is the explaination of QPO behaviour of 4U 1907+09 observations obtained 1996 February with RXTE and 1996 August with IXAE by using QPO models, and comparison of QPO results with the results of the other pulsars in which the QPOs are detected. The first QPO model was Accretion Flow Instabilities. It can be applied when the luminosity is near to the Eddington luminosity limit. And the general form of 'Eddington limit': $L_{Ed} \approx 1.3 \times 10^{38} M/M_{\odot}(\mathrm{ergs}^{-1}$. For 4U 1907+09 the Eddington limit can be written as:

$$L_{Ed} = 1.82 \times 10^{38} \mathrm{ergs}^{-1}$$

When we compare this result with observational luminosity results obtained from RXTE and IXAE.

$$L(\text{during the flare of RXTE}) = 4.0 \times 10^{36} \mathrm{ergs}^{-1}$$

$$L(\text{during the flare of IXAE}) = 3.5 \times 10^{36} \mathrm{ergs}^{-1}$$

As wee see the observed luminosities of 4U 1907+09 is below the Eddington limit, this model may not be applied to our pulsar.

Another QPO model was the KFM applied to a transient disk in 4U 1907+09. The QPOs are produced due to some inhomogeneities in the Keplerian disk that attenuate the pulsar beam regularly and the QPO (central) frequency is given by the Keplerian frequency at the inner edge of the accretion disk. From the RXTE

(1996) and IXAE (2001) observations the observed QPO frequency of the pulsar is greater than the rotation (pulse-spin) frequency of neutron star ($\simeq$ 0.00227 Hz). The observed QPO frequencies of our pulsar are (14.4 s) 0.069 Hz with IXAE and (18.2 s) 0.055 Hz with RXTE. Shortly, if the KFM works to explain the QPO production then $v_{QPO} > v_{spin}$ should be provided, otherwise no accretion will be seen in the pulsar.

One of the most plausible model among the X-ray pulsar was the Beat Frequency Model. The QPOs are produced when the material fall into the pulsar from the disk is modulated at the Keplerian frequency. According to BFM, the results of RXTE (1996) and IXAE (2001) observations are:

$$\nu_k = 0.069 + 0.00227 = 0.071\text{Hz}$$

$$\nu_k = 0.055 + 0.00227 = 0.058\text{Hz}$$

From the standard accretion disk model, the estimated Keplerian frequencies of both RXTE and IXAE observations can be written as: In IXAE observations, for a luminosity of 3.5$\times$ 10^{36} erg.s^{-1}, the μ is 9$\times$ 10^{30} Gcm^3, $v_k$$\simeq$0.071 Hz. In RXTE observations, for a luminosity of 4$\times$ 10^{36} erg.s^{-1}, the μ is 10.24$\times$ 10^{30} Gcm^3, $v_k$$\simeq$0.054 Hz.

In both models (KFM and BFM) the radius (r_d) depends on the QPO frequency and the mass of the neutron star (M). For this pulsar, r_d (disk radius) is calculated as 9.9 $\times 10^8$ cm (Makurjee et.al, 2001) which has nearly same order of magnitude as calculated in the in‘t Zand et al.1998, $\sim$ 12 $\times 10^8$ cm. This shows, for a mass of 1.4 $M_\odot$ neutron star, (r_d) are found in the range $\sim 10^8 - 10^9$ for

Table 3.2: Properties of QPOs in X-ray Pulsars

Pulsar	ν_s (mHz)	ν_{QPO} (mHz)	r_d (cm)	${\nu_k}^a$ (mHz)	${w_s}^a$	Ref.
X1626-67	130	48	1.3×10^9	178	0.73	1
GRO J1744-28	2100	400	3.1×10^8	2500	0.84	2
SMC X-1	1410	10	3.9×10^9	1420	0.99	3
X0115+63	277	62	1.1×10^9	339	0.82	4
V0332+53	229	51	1.2×10^9	280	0.82	5
Cen X-3	207	35	1.6×10^9	242	0.85	6
X Per	1.2	54	1.0×10^9	55.2	0.02	7
4U 1907+09	2.27	69	9.9×10^8	71.7	0.03	8^b
4U 1907+09	2.27	55	12.0×10^8	57.2	0.04	8^c
J1858+034	4.53	110	7.3×10^8	114.5	0.04	9
A0535+26	9.7	50	1.2×10^9	59.7	0.16	10
EXO 2030+375	24	200	4.9×10^8	224	0.11	11

[a] The quantities determined using magnetospheric beat frequency model (Alpar & Shaham 1985).
References - (1)Shinoda et al. 1990. (2)Zhang et al. 1996. (3)Angelini, Stella, & White 1991. (4)Soong & Swank 1989. (5)Takeshima et al. 1994. (6)Takeshima et al. 1991. (7)Takeshima 1997. (8^b)in't Zand et al. 1998. (8^c) Mukerjee et al. 2001. (9)Paul & Rao 1998. (10)Finger, Wilson, & Harmon 1996. (11)Angelini et al.1989.

QPO in X-ray pulsars.

In Table 3.2, the comparison of QPO parameters of 4U 1907+09 with the other X-ray pulsar having QPO with the important parameters is given (Mukerjee et.al 2001).

From this Table, we can see that the accretion disks are expected to be terminated by the strong stellar magnetic field at the radii of $10^8 - 10^9$ cm.

CHAPTER 4

RXTE OBSERVATIONS AND DATA ANALYSIS

4.1 RXTE observations

The main purpose of this thesis is to search the QPO properties of accretion powered X-ray pulsar 4U 1907+09. For searching this, the observations of 4U 1907+09 X-ray pulsar based on data collected with the RXTE-PCA (PCA: Proportional Counter Array) is used. The PCA instrument consists of an array of five proportional counters operating in the 2-60 keV, with a total collecting area of 6500 cm^2 and the field of view to 1 square degree. The observations used in this thesis according to their date are listed in Table 4.1.

Table 4.1: Journal of observations for 4U 1907+09

Time of Observation start end dd mm yyyy dd mm yyyy	XTE Obs ID
17 02 1996-23 02 1996	10155
25 11 1996-14 12 1997	10154-20146
26 07 1998-01 10 1998	30093
10 03 2001-06 03 2002	60061

These data are public and available electronically at ftp.legacy.gsfc.nasa.gov and the programmes of FTOOLS version 5.2 are used during the calculations and analysis. The data and create the main file by collecting the FS37 and FS3b knowledges in each of the data. The resulting file converted to a light curve with 1 s bins. Then power spectra from the discrete Fourier transform of every flux is formed.

In this study, we look at the 4σ and 6σ confidence levels and the above values in 0.01-0.5 frequency ranges. In some of the power spectra panels of these figures, some of 4σ and 6σ confidence levels are shown with horizontal lines. Licht curves and power spectrums can be available in Appendix A.

Figures of these QPOs with 4σ and 6σ confidence levels will be discussed in Chapter 4 and also these QPOs with 6σ confidence levels are collected as in Table 4.2, so each frequency values can be easily seen. In Table 4.2, these are given with the orbital phases and these orbital phases are calculated according to orbital epoch.

4.2 Fourier transform analysis

In getting power spectrums, the Fourier transform will be used. A Fourier transform gives a decomposition of a signal, $x(t)$, into sine waves. At any given frequency w,

$$
\begin{aligned}
x(t) &= \frac{1}{N}\sum_{j=-N/2}^{N/2-1} a_j cos(w_j t - \phi_j) = \frac{1}{N}\sum_{j=-N/2}^{N/2-1} (A_j cos(w_j t) + B_j sin(w_j t)) \\
A_j &= \sum_{k=0}^{N-1} x_k cos(w_j t) \\
B_j &= \sum_{k=0}^{N-1} x_k sin(w_j t)
\end{aligned}
$$

where A_j and B_j are Fourier coefficients where $x_k = x(t_k)$. The discrete Fourier transform $a_j(j = -N/2, ..., N/2 - 1)$ decomposes this signal into N sine waves. Here is the signal-transform pair:

$$a_j = \sum_{k=0}^{N-1} x_k e^{i2\pi jk/N} x_k = \frac{1}{N} \sum_{j=-N/2}^{N/2-1} x_k e^{-i2\pi jk/N} \tag{4.1}$$

where k=0, ..., N-1. Note that the number (N) of of input values x_k equals to number of output values a_j. The discrete form of the Parseval's theorem:

$$\sum_{k=0}^{N-1} {x_k}^2 = \frac{1}{N} \sum_{j=-N/2}^{N/2-1} {a_j}^2$$

By adopting the normalization, the power spectrum is defined as:

$$P_j \equiv \frac{2}{N_{ph}} |a_j|^2$$

where N_{ph} is the total number of photons;

$$N_{ph} = \sum_{k=0}^{N-1} x_k = a_o$$

4.3 Determination of confidence level

The power spectrum within the 0.01-0.5 Hz frequency range is normalized by using a constant value. By using this normalization for each spectrum the probability of χ^2 distribution in 2 dof is calculated; because the distribution of the P_{noise} is exactly given by this probability of χ^2 distribution in 2 dof. So that probability to exceed a certain threshold power level is given by using this χ^2 distribution. Then how large a power must be to constitute a significant excess above the noise can be determined by the χ^2 property for the noise powers.

$$\frac{\epsilon}{N_{trial}} = P\chi^2$$

where N_{trial} (number of trials) is the total number of frequencies in the range of 0.01-0.5 frequency range. (ϵ) confidence detection level defines the power level P_j due to noise and $(1-\epsilon)$ confidence level defines the power level not only due to noise but also the power level contains signal power.

Table 4.2: Time-period for 4U 1907+09 at 6σ and above confidence level

XTE Obs ID	Time day	Orbital Phase [a]	Frequency Hz
10155	10130.74528	0.521	0.0566
	10131.14533	0.568	0.036620
	10132.74759	0.760	0.036376
	10132.88664	0.776	0.035400
	10134.81893	0.007	0.042480
	10134.96507	0.024	0.037617
	10136.08180	0.158	0.054680
			0.033203
			0.036621
	10136.08903	0.158	0.034667
	10136.22878	0.175	0.056238
	10136.29029	0.182	0.033691
			0.035400
	10136.35118	0.190	0.033203
	10136.36727	0.192	0.030273
			0.034179
10154-20146	10442.07679	0.693	0.030273
			0.034423
	10443.07737	0.813	0.030517
			0.032714
			0.040039
	10477.81203	0.960	0.032226
	10567.73709	0.697	0.031005
			0.033203
	10617.42401	0.629	0.033203
	10617.49172	0.935	0.033935
	10646.64508	0.118	0.062255
	10714.48432	0.218	0.029785
	10739.35399	0.187	0.029785
			0.032470
	10796.05231	0.957	0.031250

[a] is the orbital epoch ($T_{\pi/2}$) with MJD $50134.76^{+0.16}_{-0.20}$ in 68% confidence level.

Table 4.2: (continued)

XTE Obs ID	Time day	Orbital Phase [a]	Frequency Hz
30093	11020.23164	0.724	0.039306
	11020.29539	0.732	0.067138
			0.030273
	11020.56507	0.763	0.031982
	11022.96785	0.050	0.037109
			0.042480
	11023.09835	0.066	0.029785
			0.58837
	11023.16472	0.074	0.030029
			0.033935
	11023.22769	0.082	0.034912
			0.046386
	11078.83475	0.721	0.046630
			0.054687
	11078.90100	0.729	0.039306
	11079.02815	0.744	0.050048
	11079.23058	0.768	0.032714
	11082.76096	0.190	0.030273
			0.035400
	11082.83524	0.199	0.031250
			0.036376
	11082.89377	0.206	0.042236
			0.040283
	11087.22943	0.724	0.031250
			0.032714
	11087.36658	0.739	0.033935
			0.035400
			0.036621

Table 4.2: (continued)

XTE Obs ID	Time day	Orbital Phase [a]	Frequency Hz
60061	11983.53987	0.742	0.029785
	11983.60643	0.749	0.033203
			0.035644
	11983.67529	0.758	0.040283
	12003.90723	0.173	0.032958
	12003.97818	0.182	0.049804
	12008.74589	0.751	0.032714
	12033.66487	0.727	0.033447
	12037.70885	0.210	0.030517
	12071.17703	0.206	0.032226
			0.031250
	12100.59737	0.720	0.033691
	12100.71956	0.733	0.041015
			0.043457
	12104.51962	0.186	0.029296
	12104.58588	0.195	0.031250
	12129.75718	0.200	0.044921
	12134.37726	0.752	0.044433
	12159.41921	0.742	0.044433
	12205.10156	0.196	0.049560
			0.052246
	12205.12656	0.199	0.030273
	12205.17454	0.205	0.031982
	12234.75400	0.736	0.040527
	12271.85903	0.167	0.031250
			0.035400
	12276.81707	0.759	0.030273
			0.036865
			0.047714
	12309.99848	0.721	0.041015

CHAPTER 5

DISCUSSION AND CONCLUSION

In the last part of this study, the results of these analysis of 4U 1907+09 will be discussed.

To see the distribution of the QPOs with 4σ confidence level, we have to look at behaviour of QPOs according to the orbital phase as in Figure 5.1. QPOs are mostly collected near the phases of 0.2 and 0.7. In other phases, no QPO frequency values or few are detected. The observed data of 4U 1907+09 with PCA and also the QPO frequency detected in 1997 with RXTE, 0.054 Hz, can also be seen in Figure 5.1 (upper panel). To look at these QPOs data in more detail, we also look at the distribution of frequency values with 6σ and the above confidence level. We get the same result, and the QPOs distribute near the phases of 0.2 and 0.7, also 0.054 Hz of QPOs can be seen in Figure 5.1 (lower panel) (All the frequency values for each orbital phases can be seen in detail in Table 4.2).

During the study, the QPO frequencies which are above the 6σ confidence level are used. Firstly we take the light curve of QPOs according to phases by using PCA (For data, see Table 4.1). With RXTE-PCA, we can make a decision about the behaviour of the neutron star around its companion star in every cycle. Here we can see the highest count rates collected near the orbital phases in which the

QPOs can be seen mostly (see Figure 5.2 (upper panel)). From pervious analysis, we know that this source shows two flares in every cycle while the neutron star passes through the Be star equatorial wind.

We use the time spans associated with PCA observation data by using All-Sky Monitor (ASM consists of three wide-angle shadow cameras equipped with Xenon proportional counters in the 2-10 keV, with a total collecting area of 90 cm^2. The instrument's time resolution is 80 % of the sky in every 90 minutes). And we get Figure 5.2 (lower panel) and from this figure we can see that we get two peaks in every cycle as it should be.

4U 1907+09 has persistent spin down trend since 1983 and with this study we have seen the QPO trends through the flares persistent in this source and the persistent QPO behaviour which is greater than spin frequency strongly suggest that this source has an accretion disk which forms around its Be type companion star. Future observations may give information about QPO trends around other orbital phases.

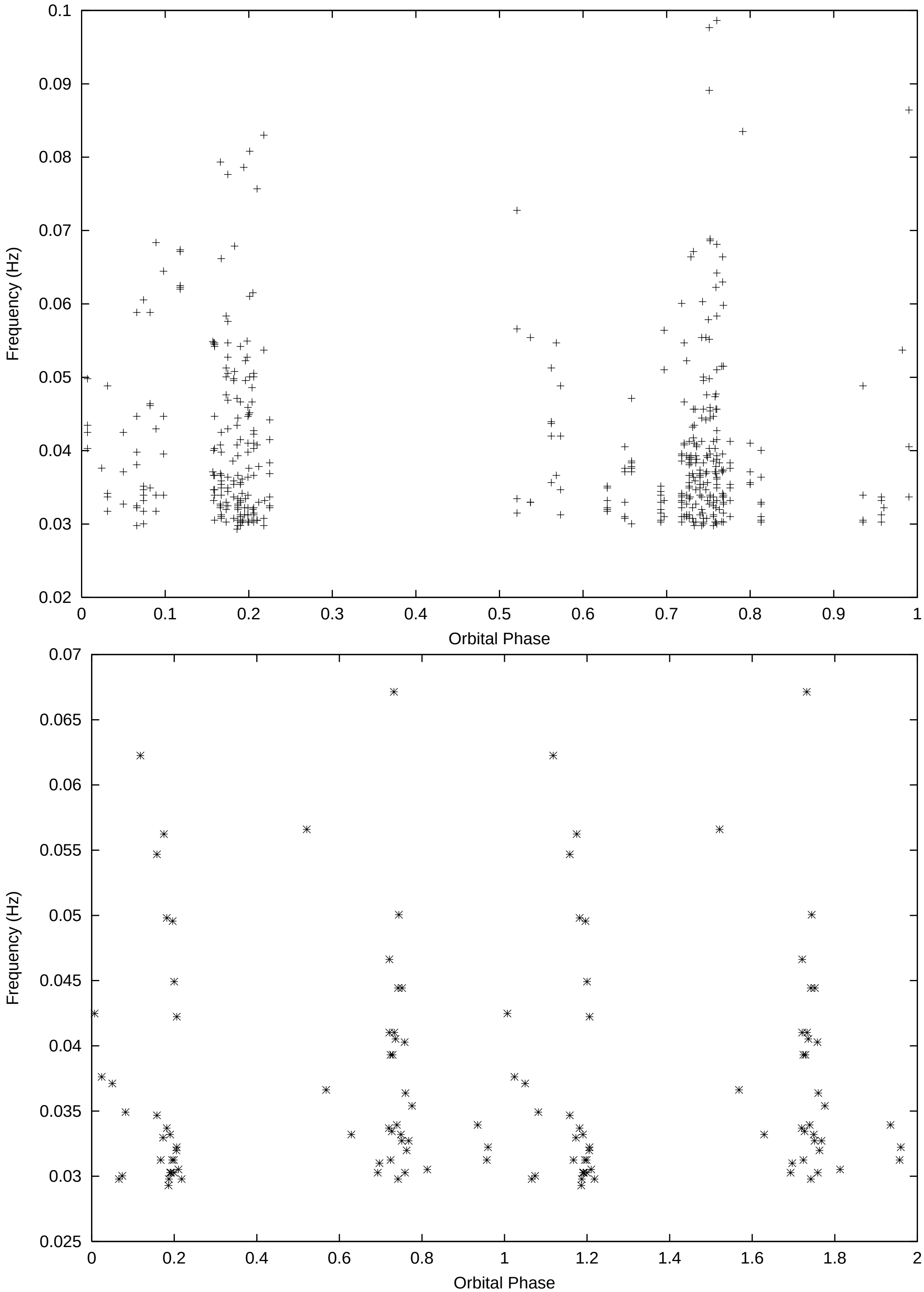

Figure 5.1: Frequency versus Orbital Phase for 4σ (upper panel) and 6σ (lower panel) values

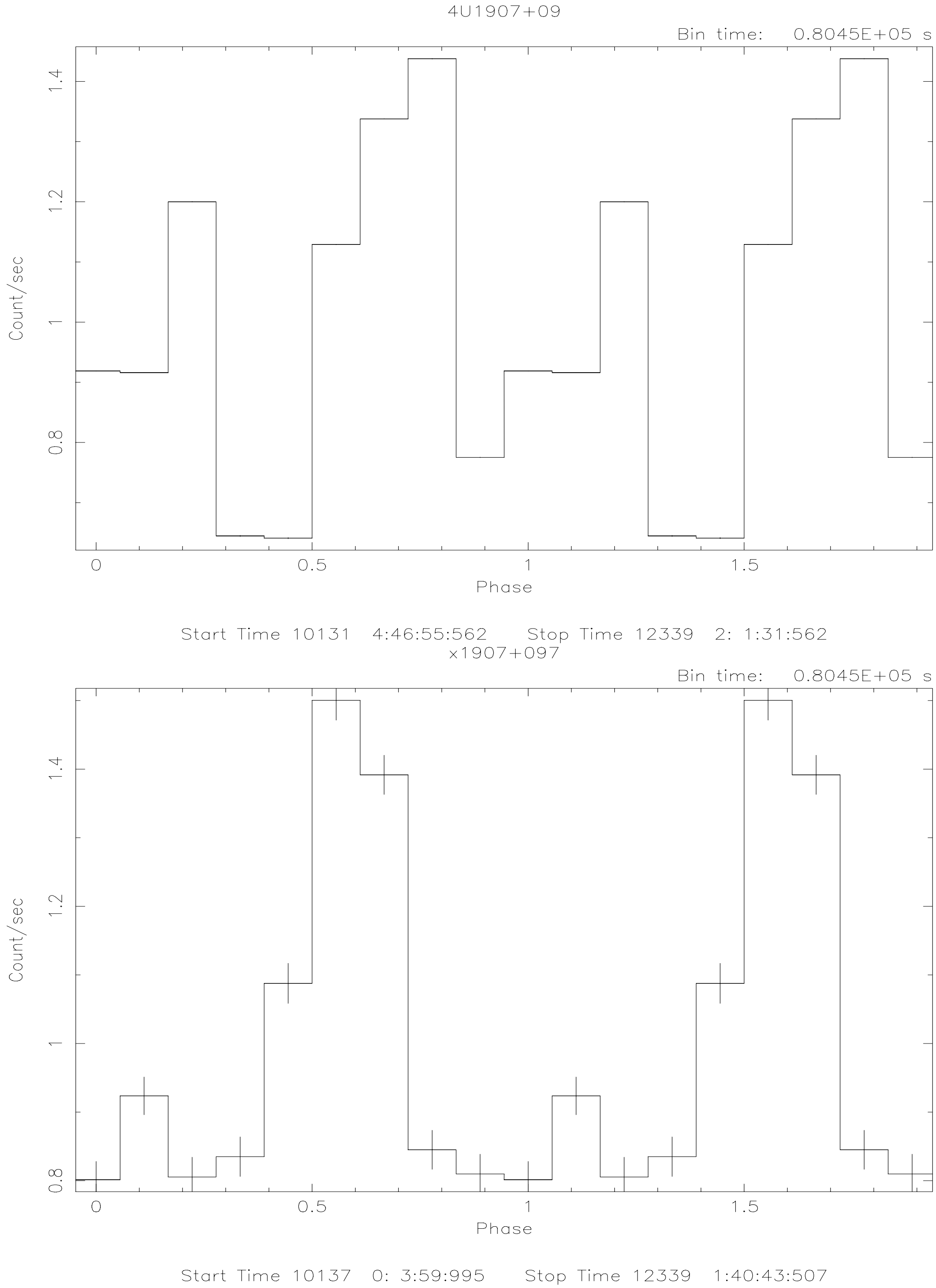

Figure 5.2: Count rate in RXTE-PCA (upper panel) and ASM (lower panel) versus Orbital Phase.

REFERENCES

[1] Alpar, M.A., Shaham, J. 1985, Nature, 316, 239

[2] Angelini L., Stella, L., Parmar, A.N. 1989, ApJ, 346, 906

[3] Angelini L., Stella, L., White, N.E. 1991, ApJ, 371, 332

[4] Anzer, U., Börner G. 1980, A&A, 83,133

[5] Baykal, A. et al. 2001, ApJ, 327, 1269

[6] Bildsten, L. et al. 1997, ApJSS, 113, 367

[7] Boronson, B. et al. 2000, ApJ, 545, 399

[8] Chakrabarty, D. 1996, Ph.D Thesis submitted to California Institute of Technology

[9] Cook, M.C., Page, C.G. 1987, MNRAS, 225, 381

[10] Corbet, R.H.D. 1984, A&A, 141, 91

[11] Corbet, R.H.D. 1986, MNRAS, 220, 1047

[12] Cui, W. 1997, ApJ, 482, L163

[13] Davidson, K., Ostriker, J.P. 1973, ApJ, 179, 585

[14] Finger et al. 1996, A&A, 120, 209

[15] Fronter, B. et al. 1989, Nature, 342, 775

[16] Ghosh, P., Lamb, F.K. 1978, ApJ, 223, L83

[17] Ghosh P., Lamb, F.K. 1979a, ApJ, 232, 259

[18] Ghosh P., Lamb, F.K. 1979b, ApJ, 234, 296

[19] Giacconi, R. et al. 1962, Phys. Rev. Lett., 9, 439

[20] Giacconi, R. et al. 1971, ApJ, 165, L27

[21] Guseinov, O.H. et al. 2000, AstL, 26, 725

[22] Hasinger, G., van der Klis, M. 1989, A&A, 225, 79

[23] Int't Zand, J.J.M., Baykal, A., Strohmayer, T.E. 1998, ApJ, 496, 386

[24] Int't Zand, J.J.M., Strohmayer, T.E., Baykal, A. 1997, ApJ, 479, L47

[25] Iye, M. 1986, PASJ, 38, 463

[26] Kommers, J.M. et al. 1998, ApJ, 497, L33

[27] Lamb, F.K. 1988, Adv. Space Res., 8, 421

[28] Lamb, F.K. et al. 1973, ApJ, 184,271

[29] Lipunov, Vladimir M. 1992, Astrophysics of Neutron Star

[30] Liu, Q.Z. et al. 2000, A&A SS, 142, 25-49

[31] Makishima, K. et al. 1984, PASJ, 36, 679

[32] Makurjee, K. et al. 2001, ApJ, 548, 368

[33] Marshall, N., Ricketts, M.J. 1980, MNRAS, 193, 7P

[34] Mihara, T. 1995, Ph.D. Thesis, Univ. Tokyo

[35] Moon, D., Eikenberry, S.S. 2001, ApJ, 549, L225

[36] Motch, C. et al. 1991, ApJ, 369, 490

[37] Nagase, F. 1989, PASJ, 41, 1

[38] Nelson, R.W. et al. 1997, ApJ, 488, L117

[39] Paul, B., Rao, A.R. 1998, ApJ, 337, 815

[40] Pringle, J.E., Rees M.J., 1972, A&A, 21, 1

[41] Reig, P., Roche, P. 1999, MNRAS, 306, 100

[42] Scott, D.M. et al. 1997, ApJ, 488, 831

[43] Shinoda, K. et al. 1990, PASJ, 42, L27

[44] Soong, Y., Swank, J.H. 1989, The 23rd ESLAB Symposium on Two Topics in X-ray Astronomy . Vol 1: X-ray Binaries, 617

[45] Stella, L. et al. 1986, ApJ, 308, 669

[46] Takeshima, T. et al. 1991, PASJ, 43, L43

[47] Takeshima, T. et al. 1994, ApJ, 436, 871

[48] Takeshima, T. 1997, BAAS, 191, 111

[49] van der Klis, M. 1988, in Timing Neutron Stars, NATO Advanced Study Institue, ed. H.Ögelman and E.P.J van der Heuvel (Kluwer Academic Publishres, Dordrecht), 28-42

[50] van der Klis, M. 1993, X-Ray Binaries, eds. W.H.G.Lewin et al., 279-284

[51] White, N.E. et al. 1993, X-Ray Binaries, eds. W.H.G.Lewin et al., 1-57

[52] Zhang, W. et al. 1996, ApJ, 469, L29

APPENDIX A

Light curves and power spectra

The light curves and power spectra done in this study are presented in this part of the thesis. In every page, the light curves and the related power spectrum are positioned respectively in the left side and towards to the right side of the page. Mainly in each pages in every row there are four figures.

In these configurations, the figures are arranged according to their date and the oldest datum's figures are positioned on the top of the left side of the page and the next datum's figures are postioned below of this oldest datum's figures.

Some light curves have two power spectra instead of another light curve and power spectrum pair in one row; in page 52 the second line,in page 59 the first line, in page 63 the last 3 lines, in page 64 the first and the last lines, in page 65 the fifth line, in page 67 the first line.

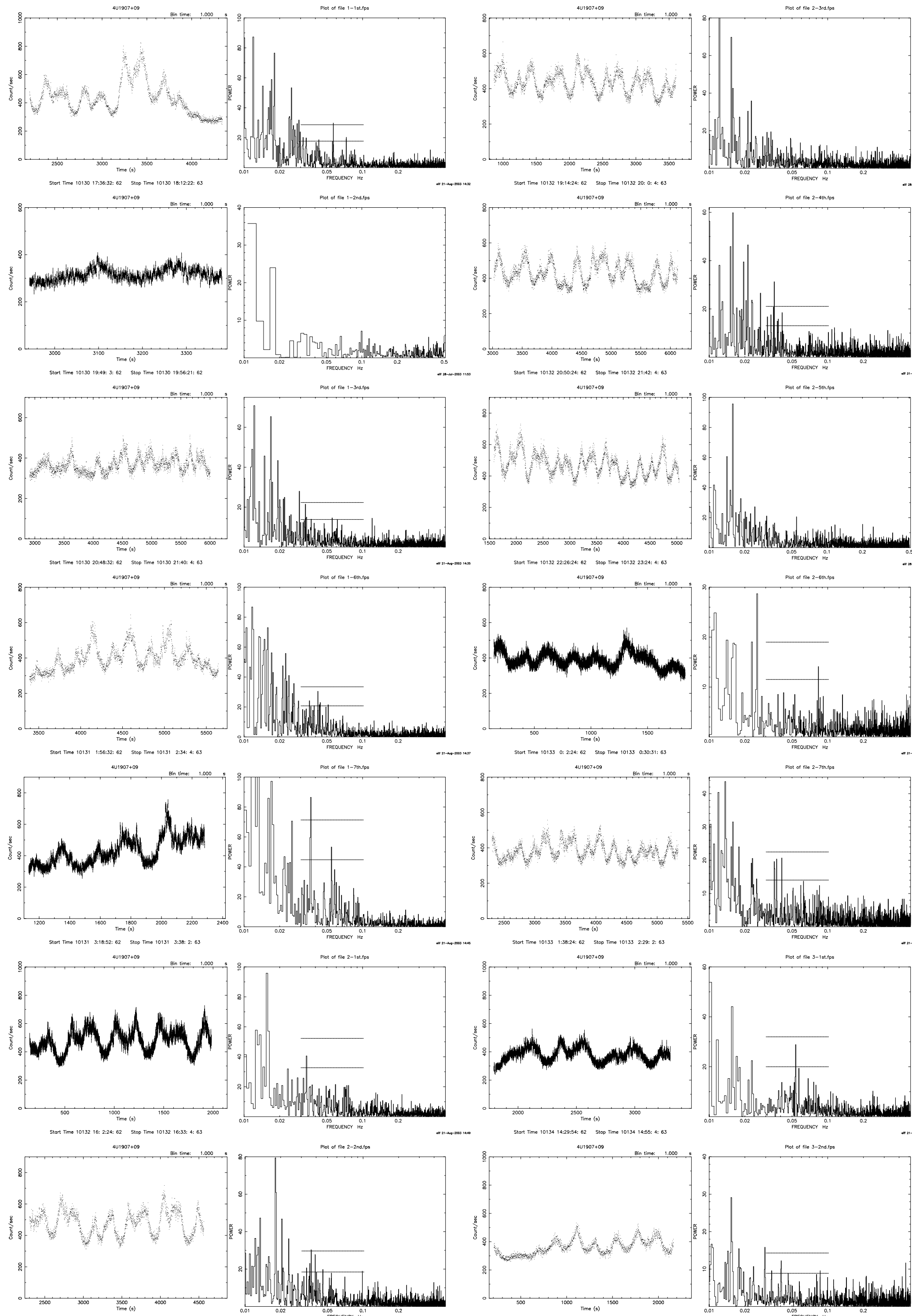

Figure A.1: Light curves and power spectra of 10155

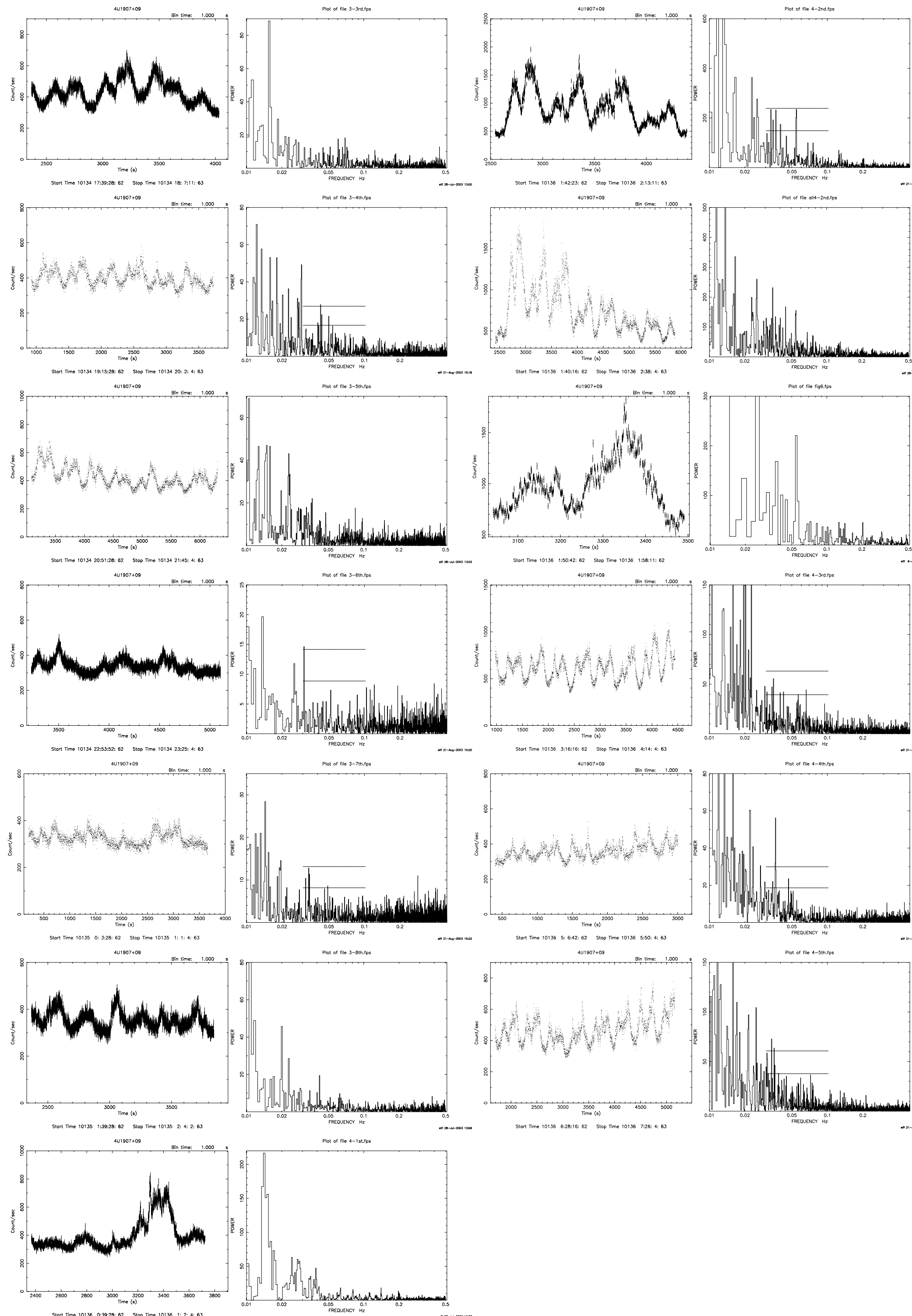

Figure A.1: (continued)

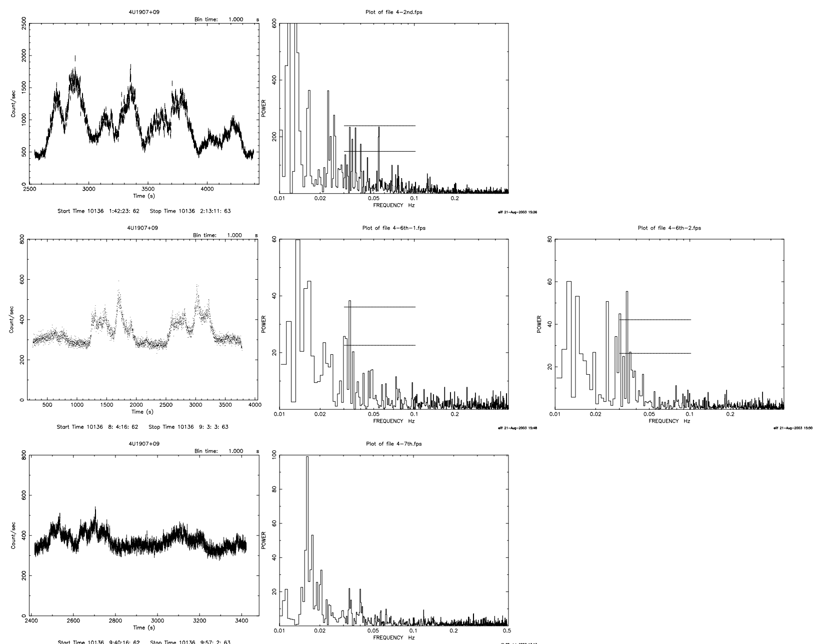

Figure A.1: (continued)

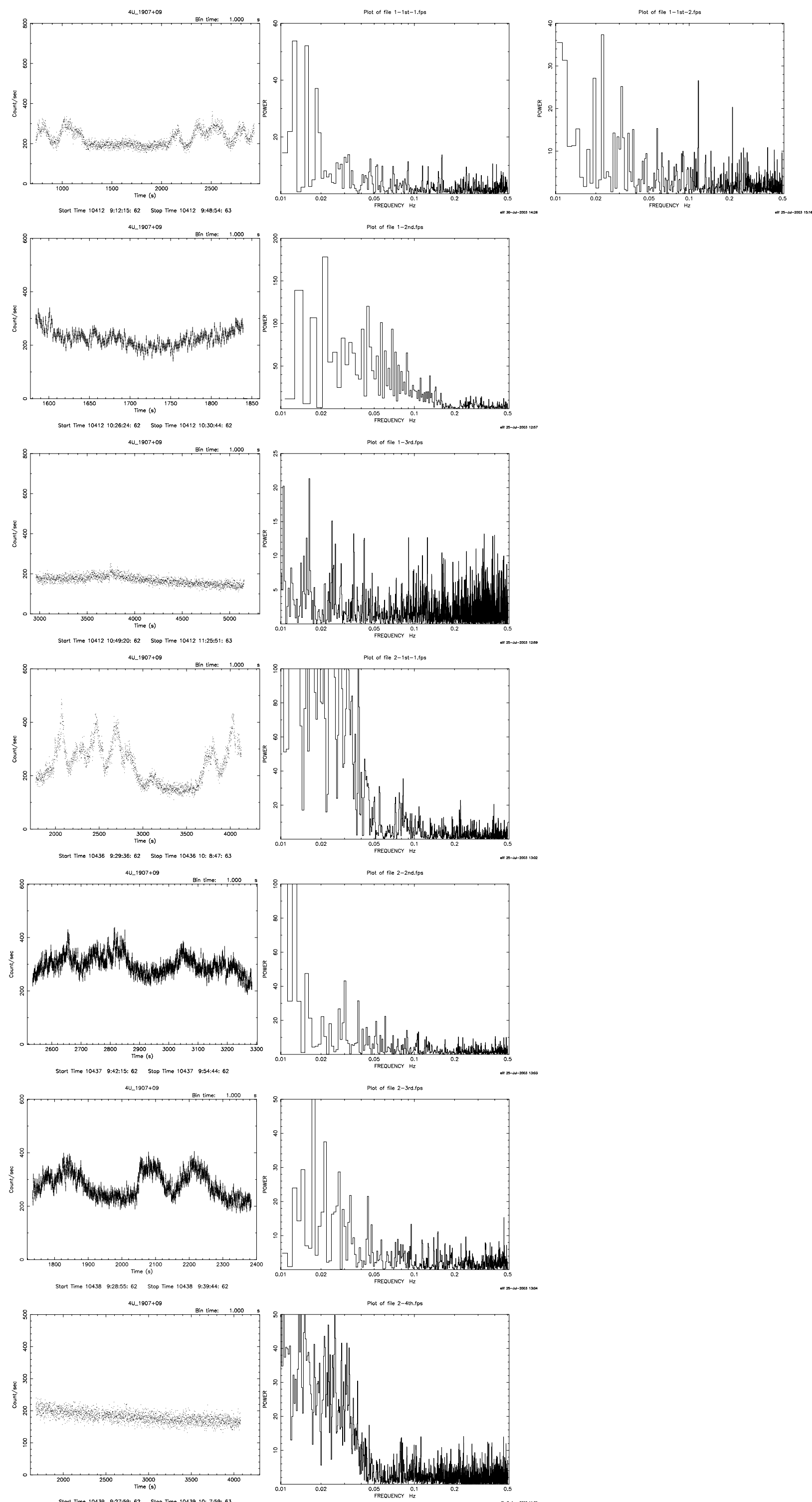

Figure A.2: Light curves and power spectra of 10154

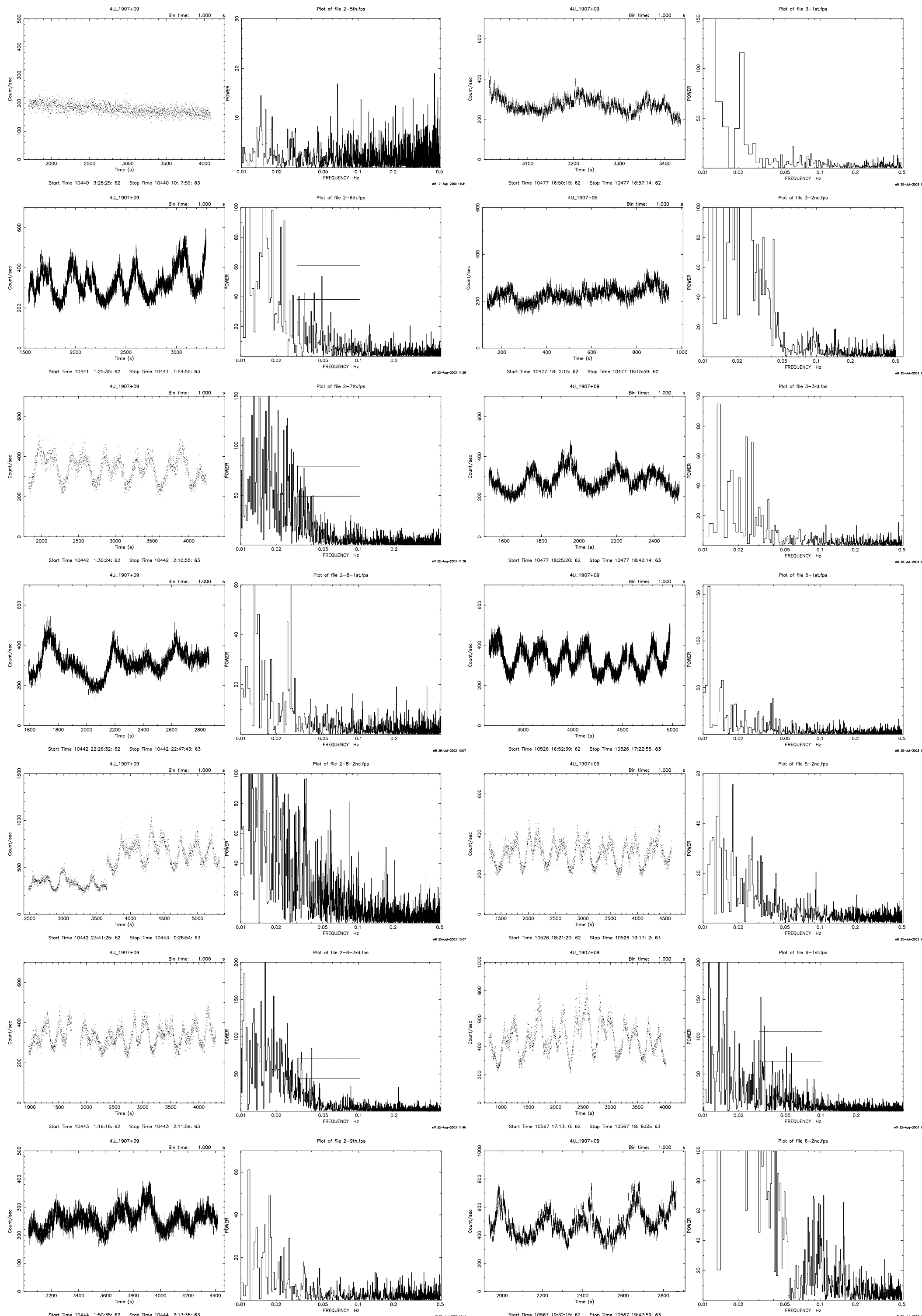

Figure A.2: (continued)

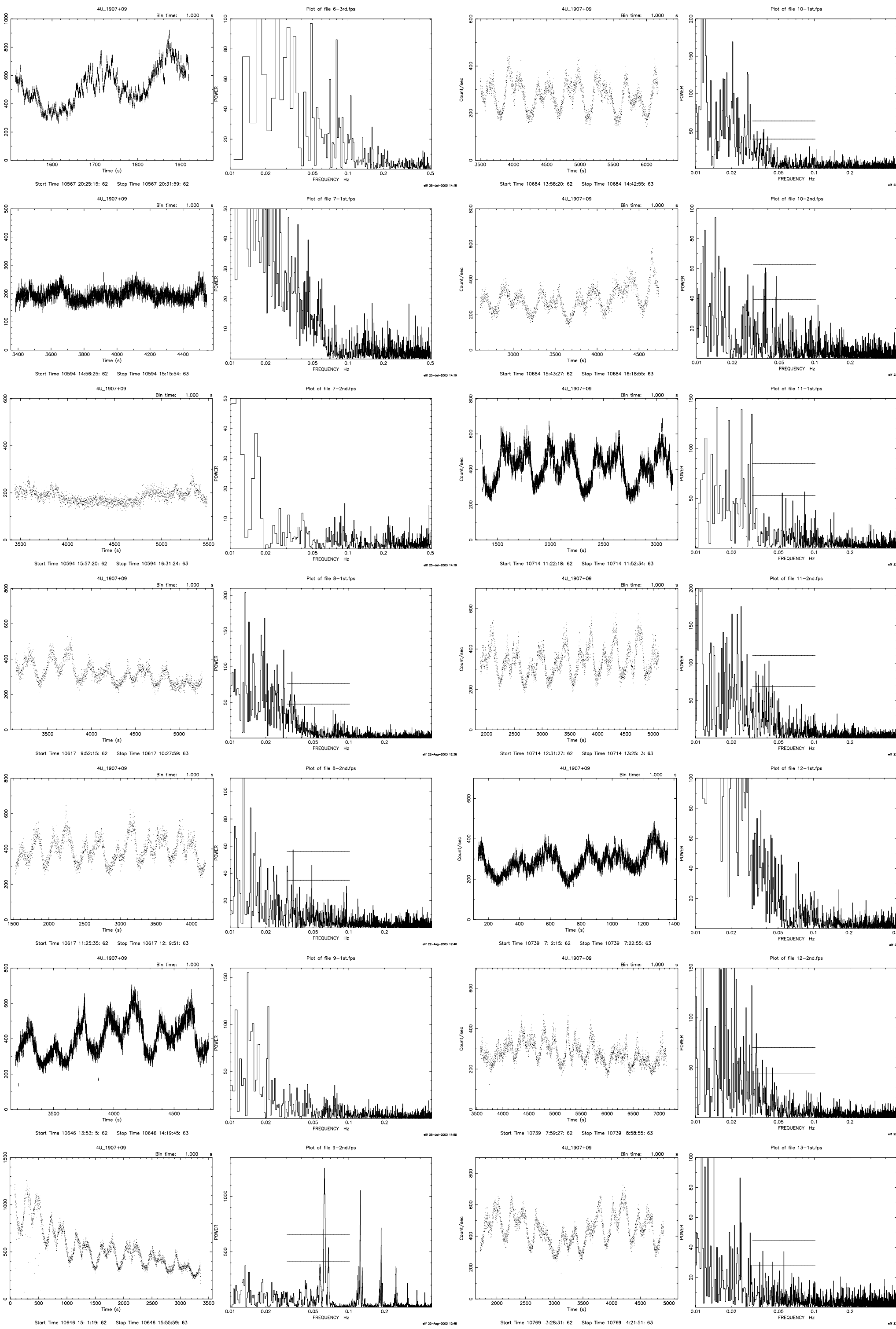

Figure A.2: (continued)

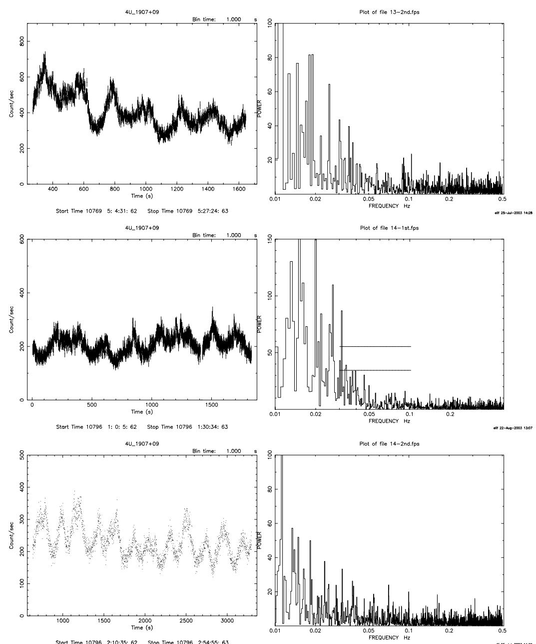

Figure A.2: (continued)

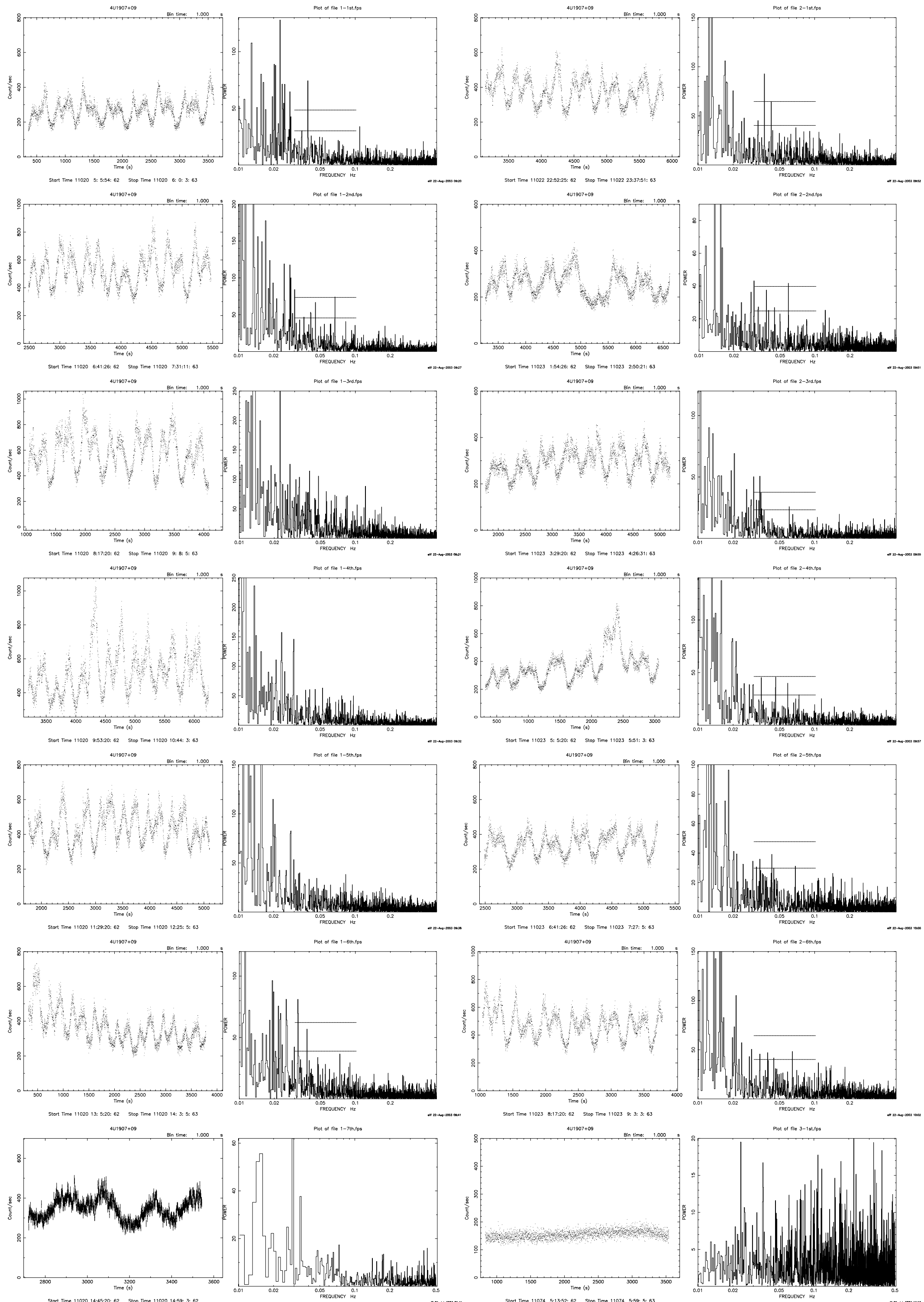

Figure A.3: Light curves and power spectra of 30093

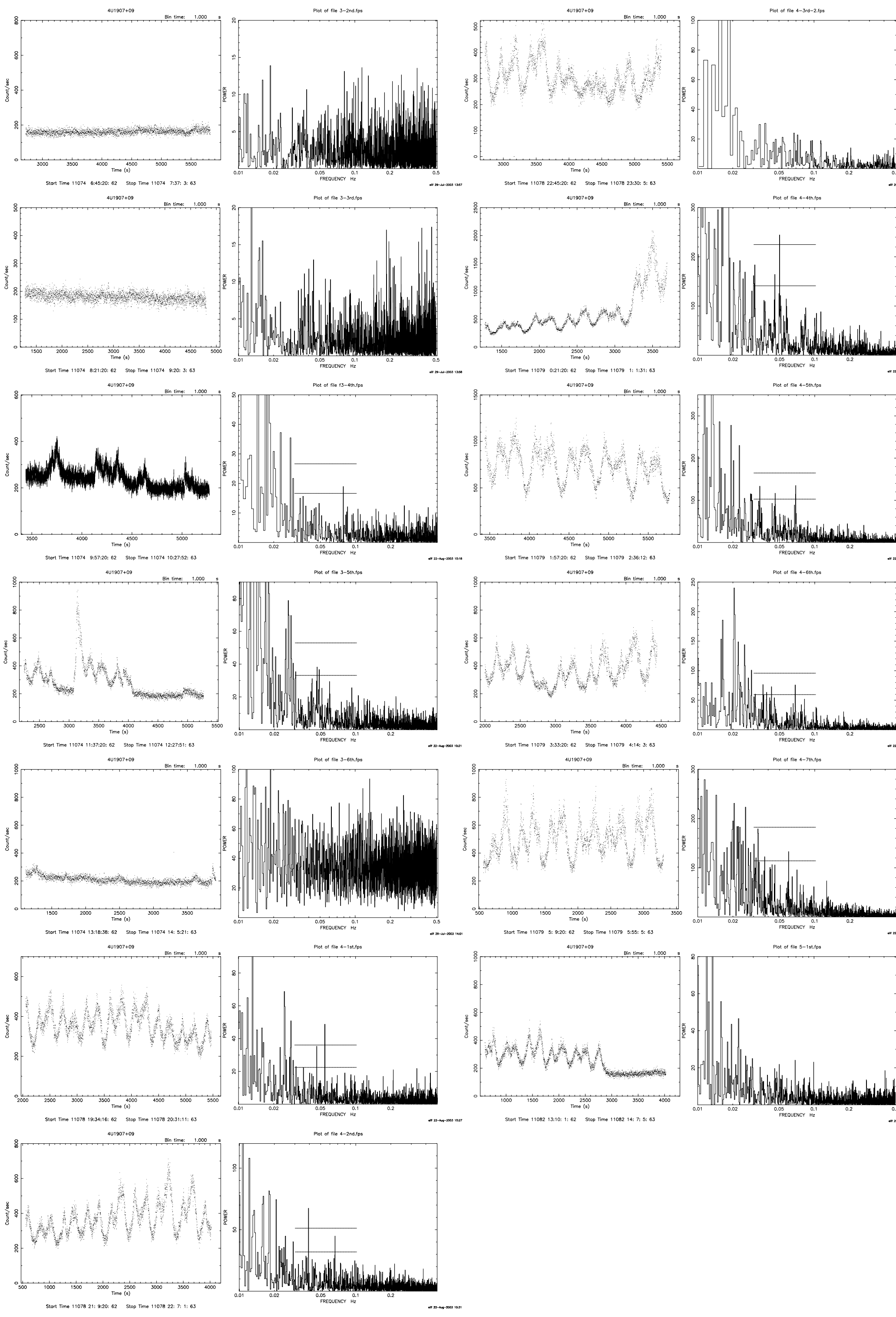

Figure A.3: (continued)

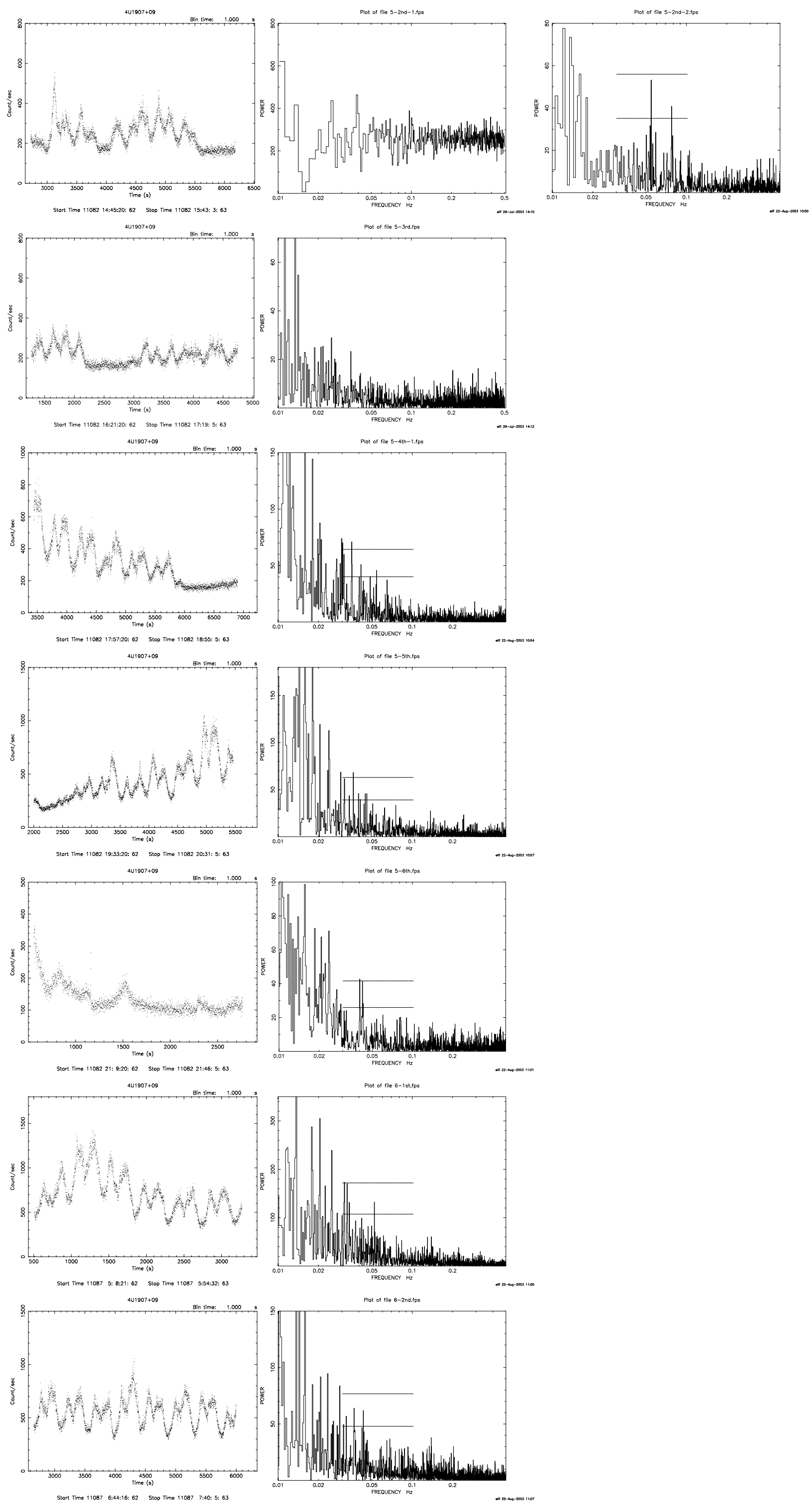

Figure A.3: (continued)

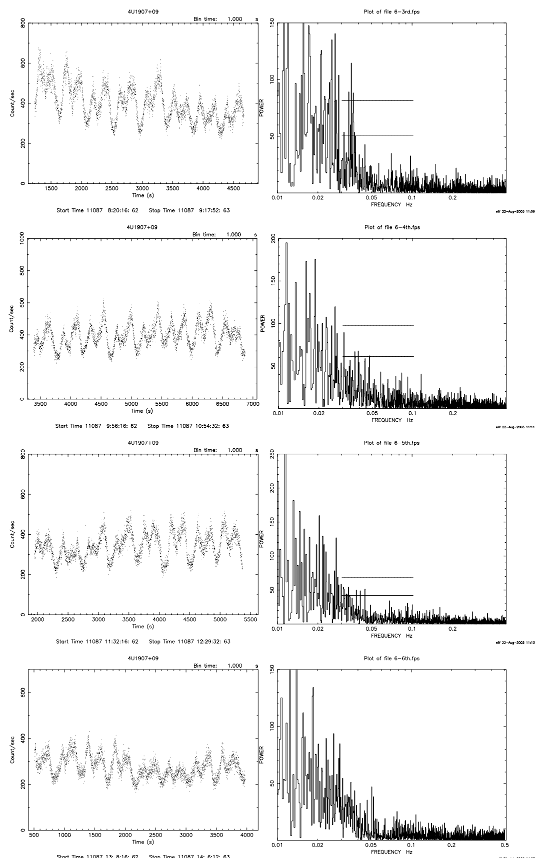

Figure A.3: (continued)

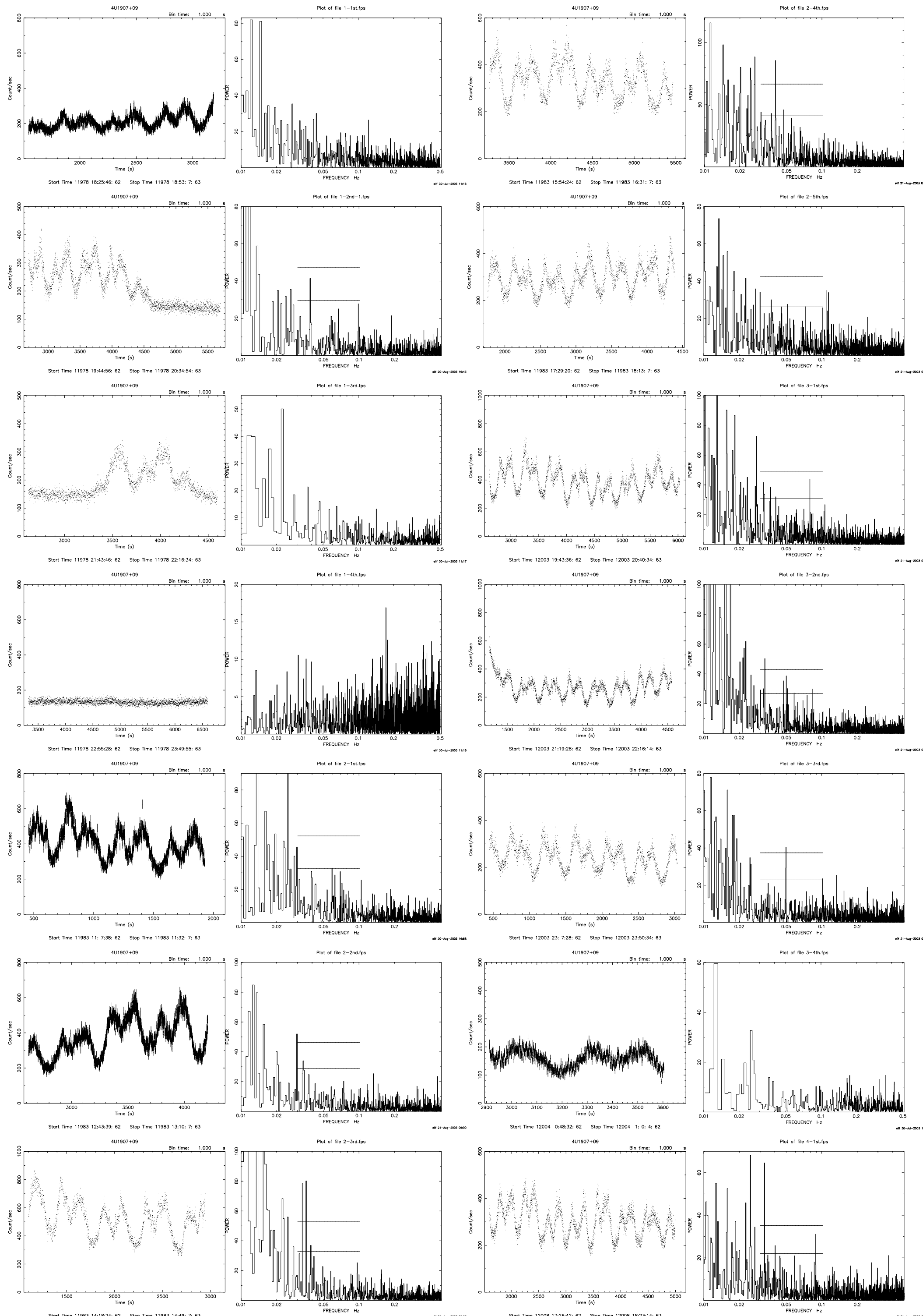

Figure A.4: Light curves and power spectra of 60061

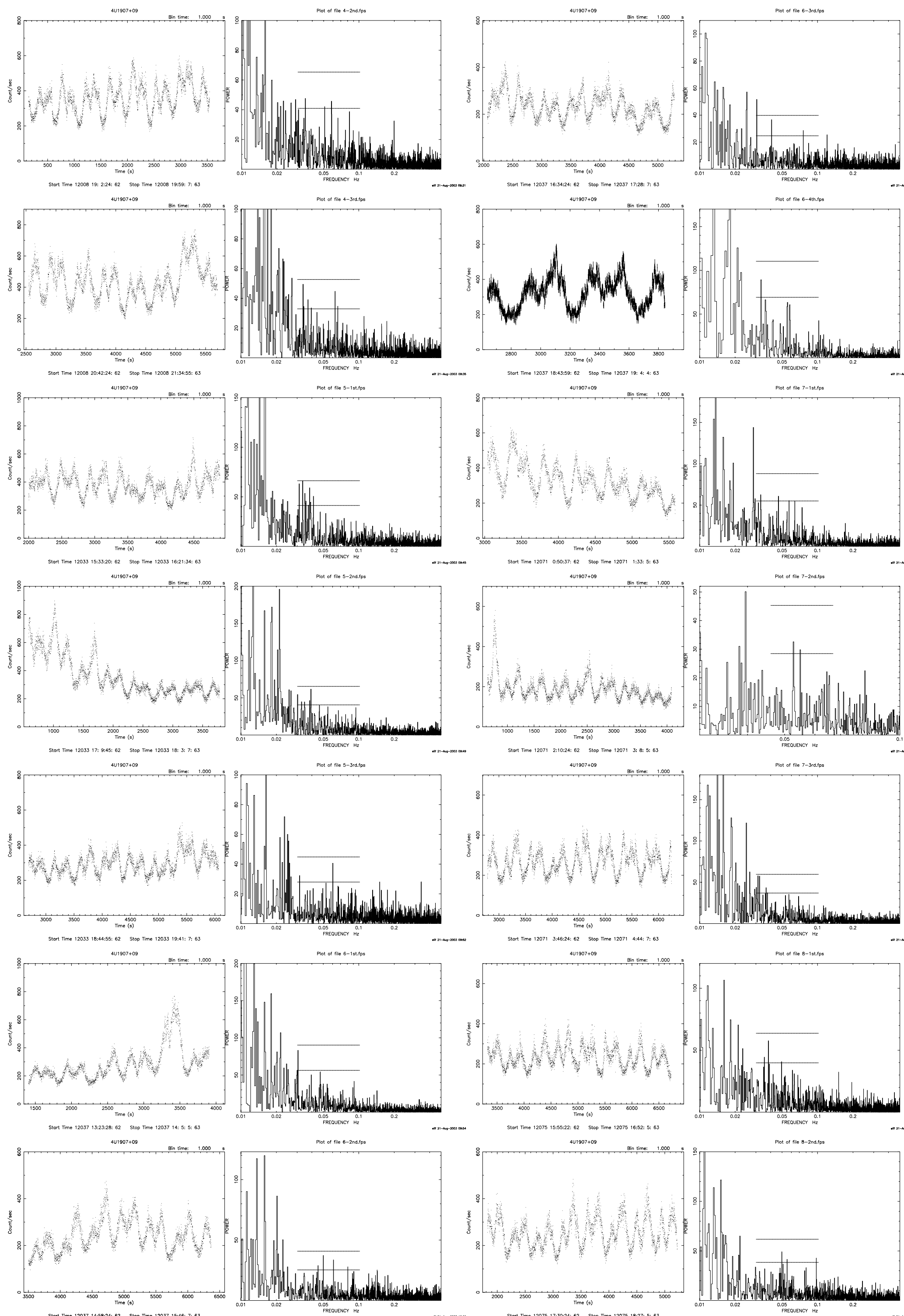

Figure A.4: (continued)

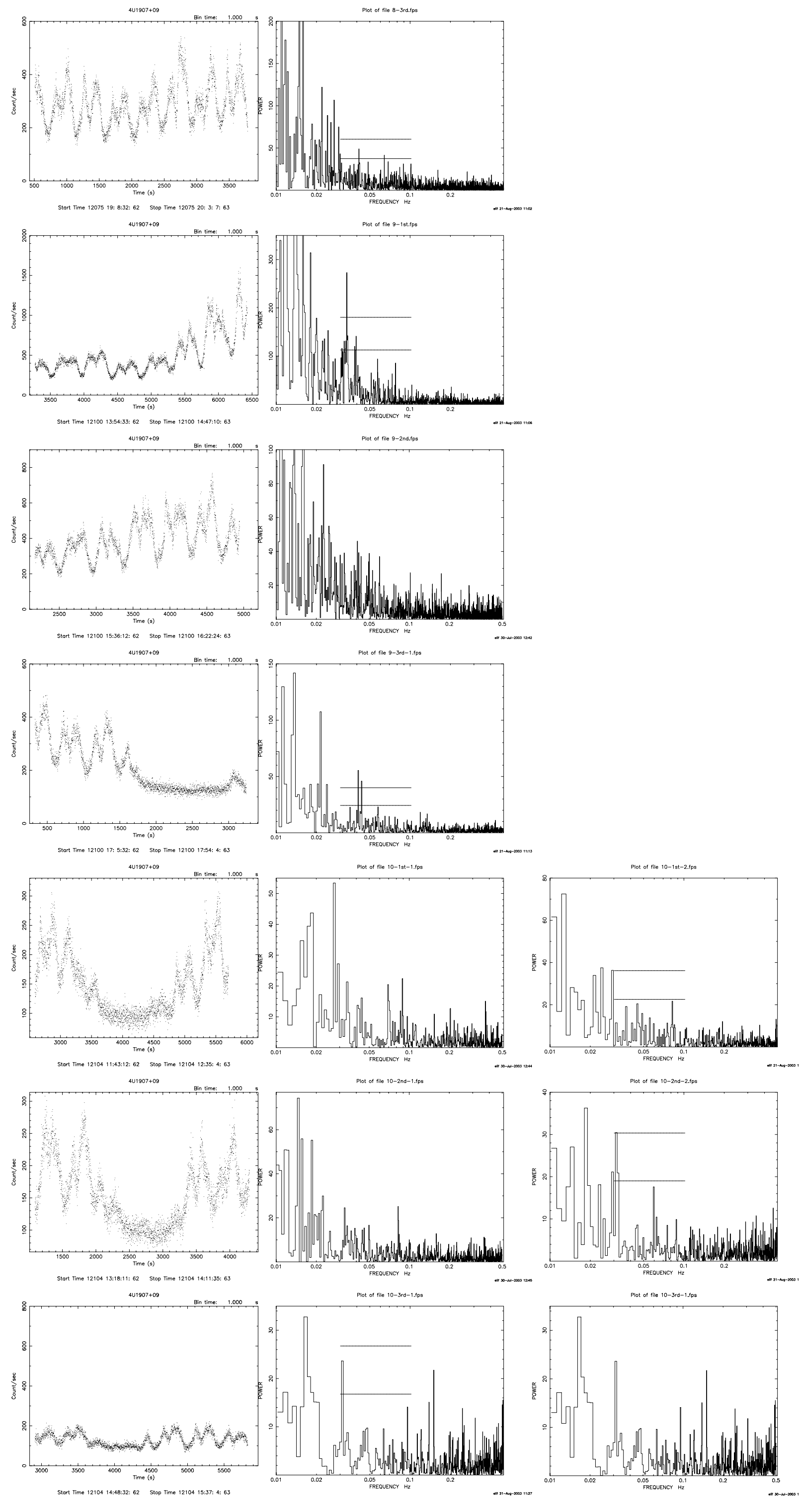

Figure A.4: (continued)

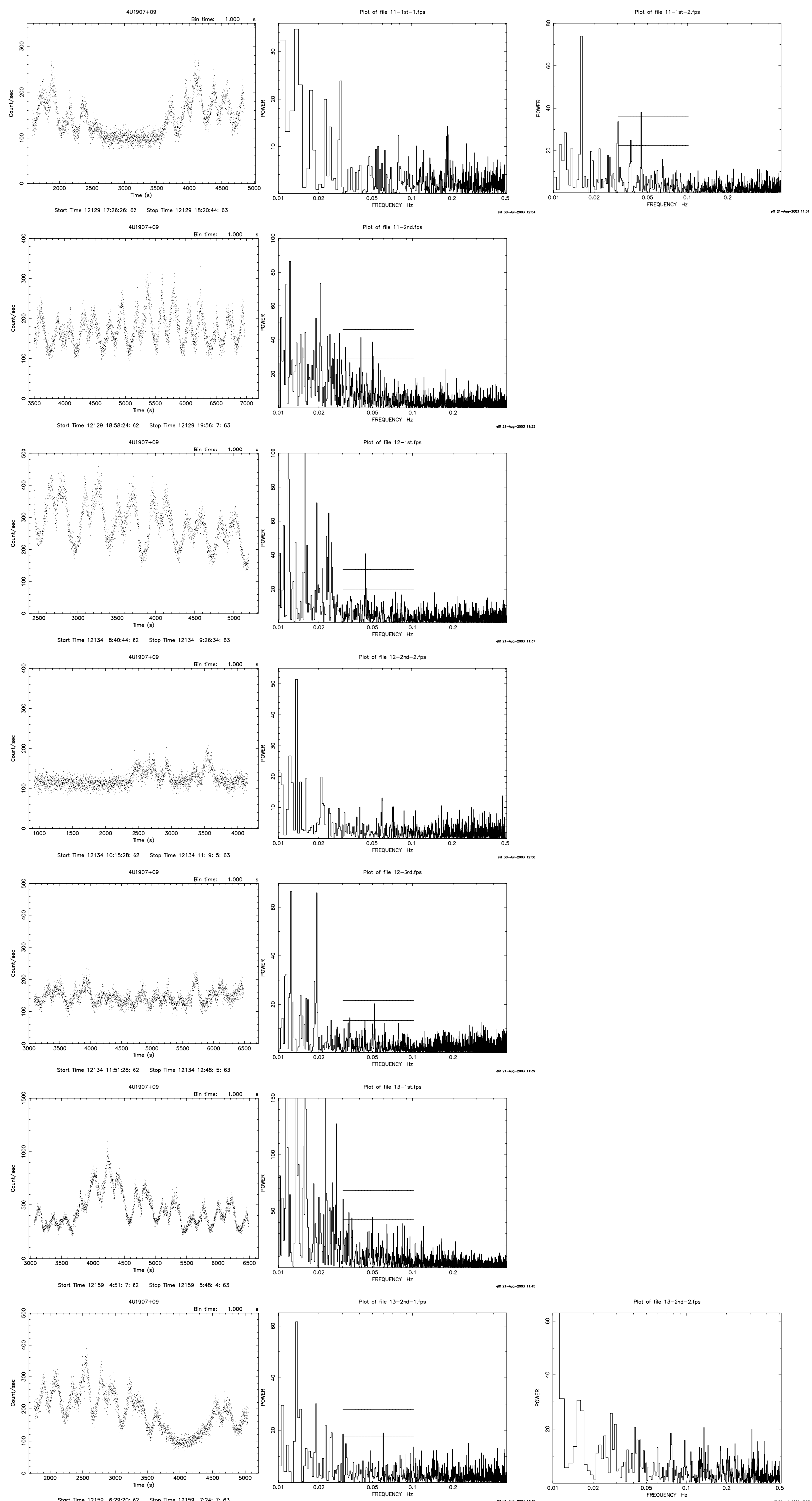

Figure A.4: (continued)

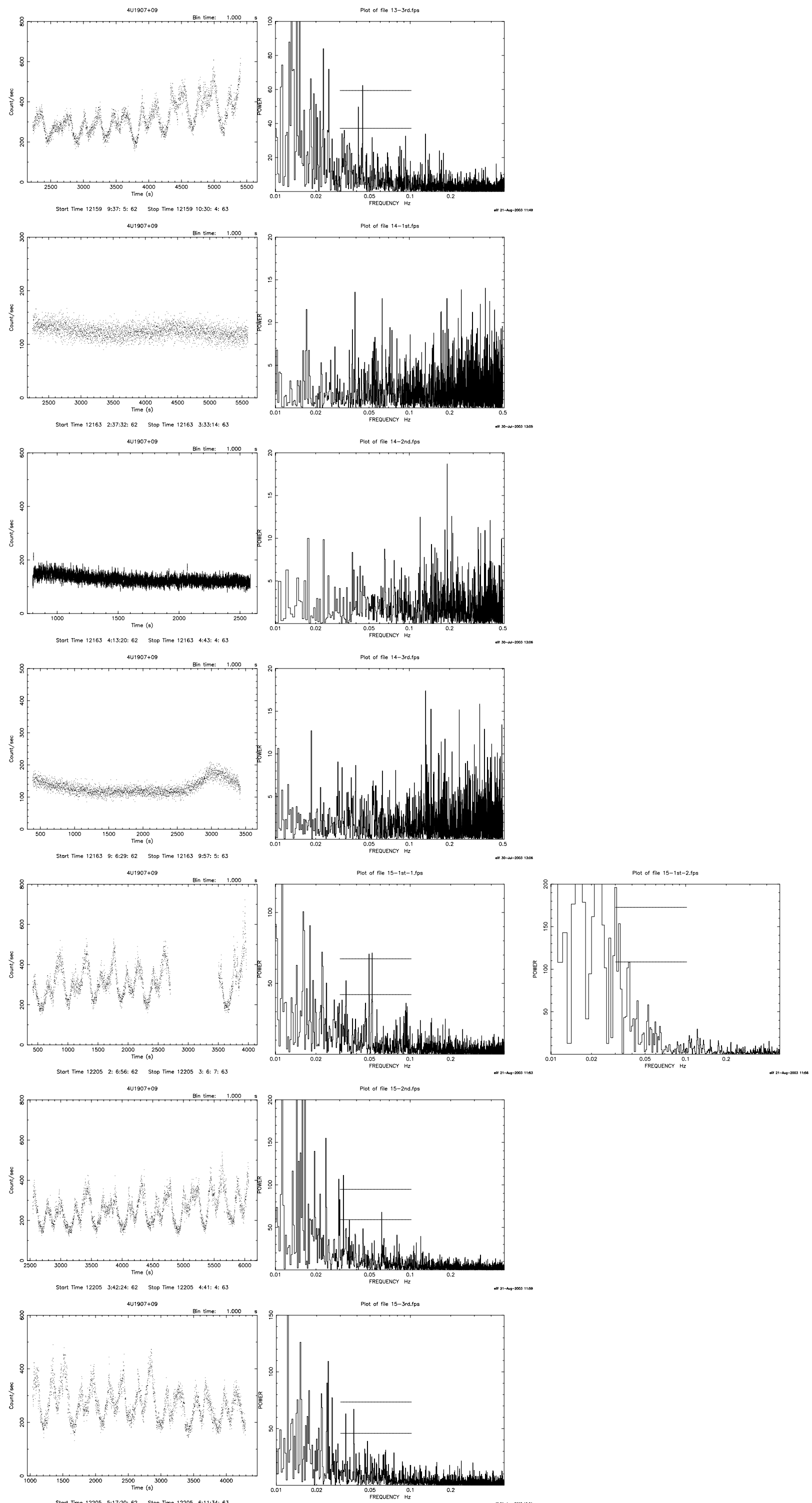

Figure A.4: (continued)

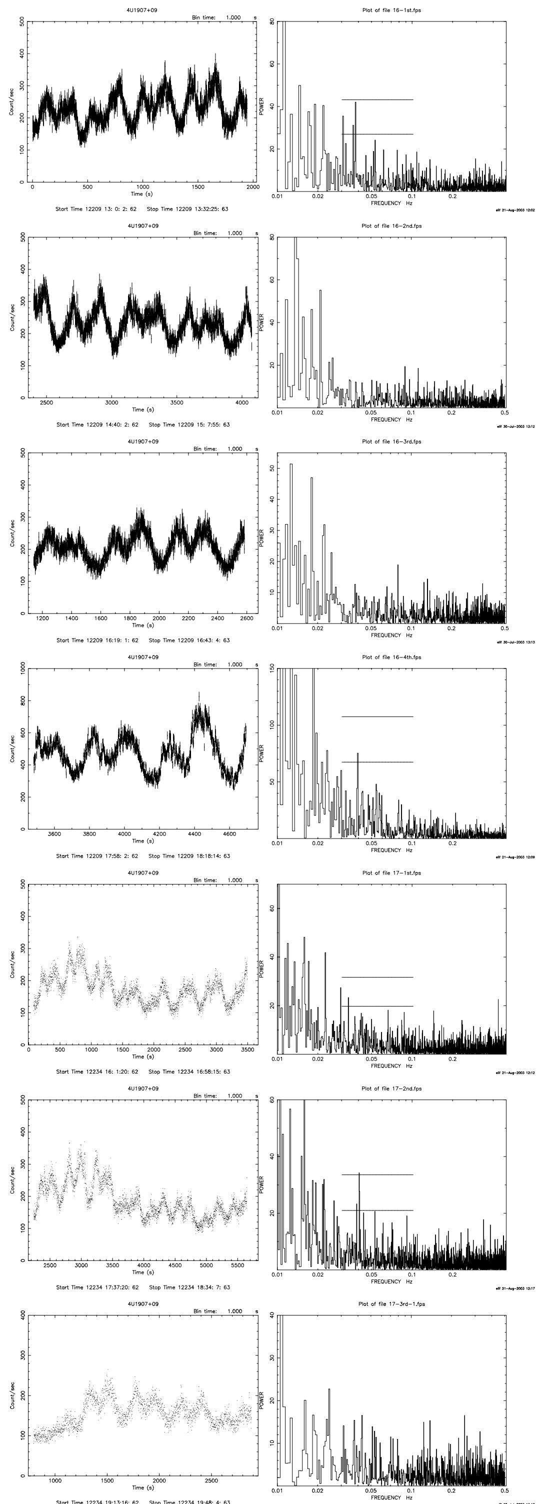

Figure A.4: (continued)

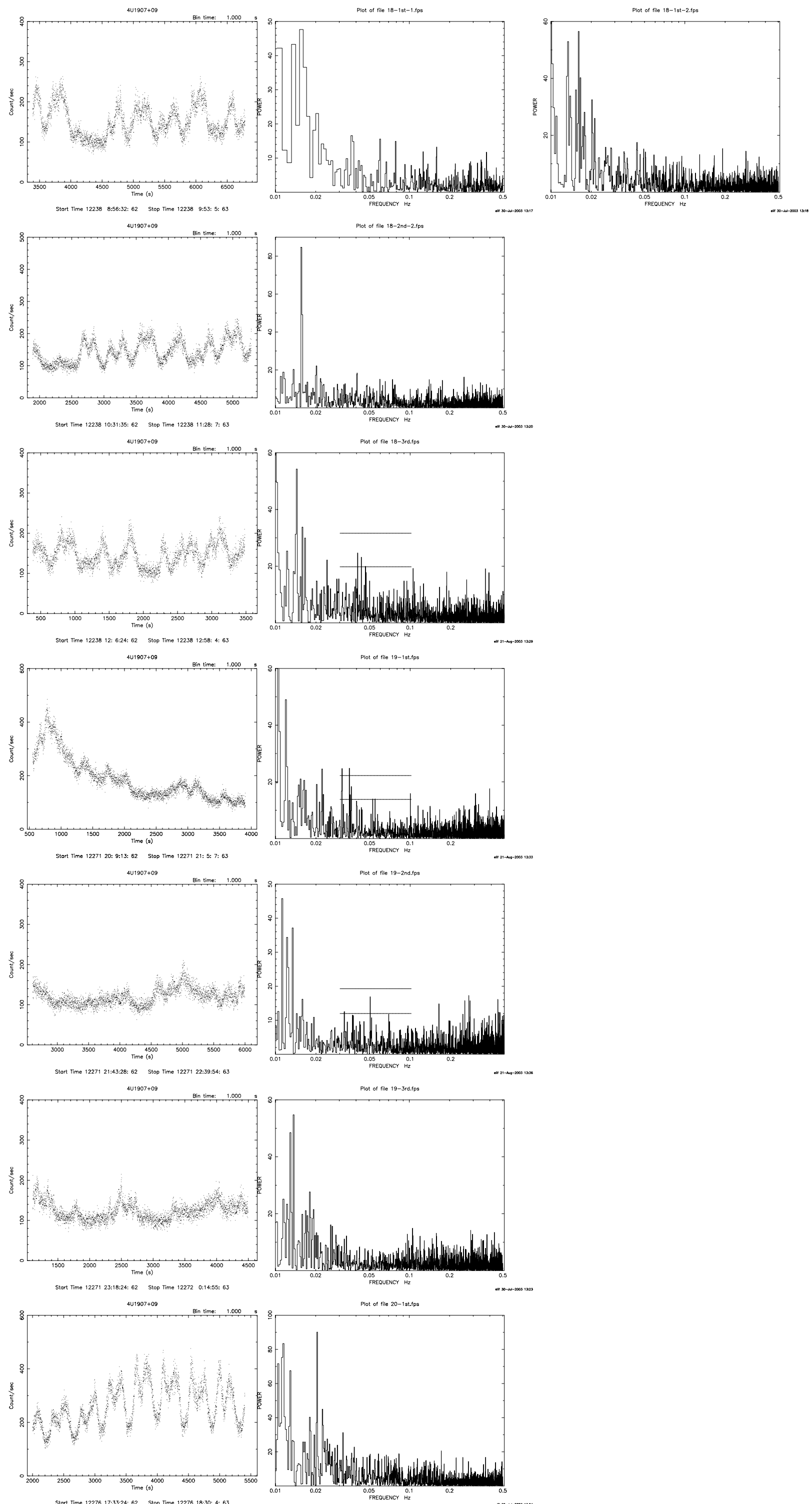

Figure A.4: (continued)

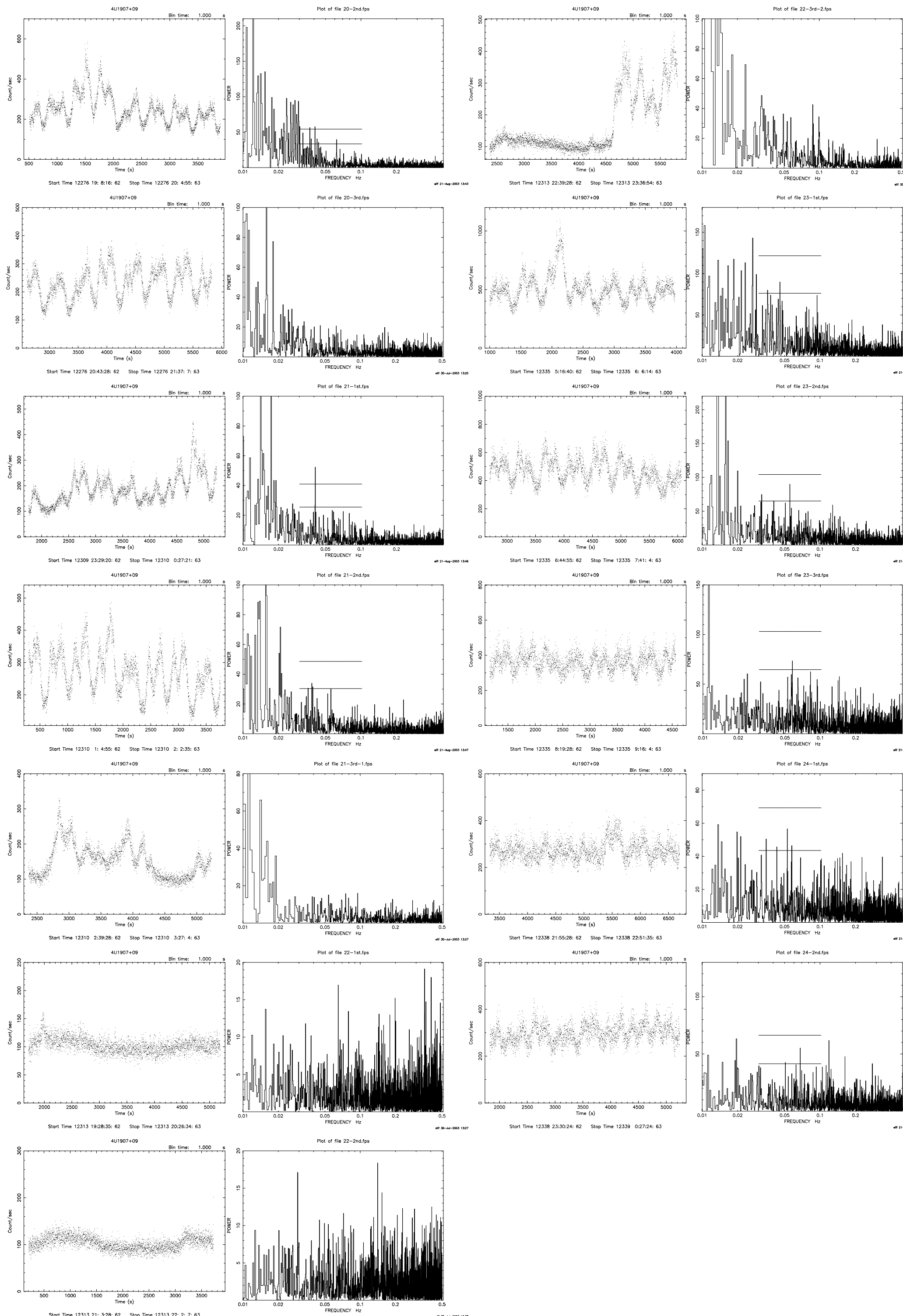

Figure A.4: (continued)